

Data-Driven Deep MIMO Detection: Network Architectures and Generalization Analysis

Yongwei Yi, Xinping Yi, *Member, IEEE*, Wenjin Wang, *Member, IEEE*,
Xiao Li, *Member, IEEE*, and Shi Jin, *Fellow, IEEE*

Abstract—In practical Multiuser Multiple-Input Multiple-Output (MU-MIMO) systems, symbol detection remains challenging due to severe inter-user interference and sensitivity to Channel State Information (CSI) uncertainty. In contrast to the mostly studied belief propagation-type model-driven methods, which incur high computational complexity, Soft Interference Cancellation (SIC) strikes a good balance between performance and complexity. To further address CSI mismatch and nonlinear effects, the recently proposed data-driven deep neural receivers, such as DeepSIC, leverage the advantages of deep neural networks for interference cancellation and symbol detection, demonstrating strong empirical performance. However, there is still a lack of theoretical underpinning for why and to what extent DeepSIC could generalize with the number of training samples.

This paper proposes inspecting the fully data-driven DeepSIC detection within a Network-of-Multi-Layer Perceptrons (MLPs) architecture, which is composed of multiple interconnected MLPs via outer and inner Directed Acyclic Graphs (DAGs). Within such an architecture, DeepSIC can be upgraded as a graph-based message-passing process using Graph Neural Networks (GNNs), termed GNNSIC, with shared model parameters across users and iterations. Notably, GNNSIC achieves excellent expressivity comparable to DeepSIC with substantially fewer trainable parameters, resulting in improved sample efficiency and enhanced user generalization. By conducting a norm-based generalization analysis using Rademacher complexity, we reveal that an exponential dependence on the number of iterations for DeepSIC can be eliminated in GNNSIC due to parameter sharing. Simulation results demonstrate that GNNSIC attains comparable or improved Symbol Error Rate (SER) performance to DeepSIC with significantly fewer parameters and training samples.

I. INTRODUCTION

MULTIUSER Multiple-Input Multiple-Output (MU-MIMO) has been a cornerstone technology for wireless communication systems, meeting the rapidly increasing throughput demands of modern wireless services. In uplink cellular networks, base stations equipped with multiple antennas can simultaneously serve multiple user terminals by exploiting spatial multiplexing, enabling significant improvements in spectral efficiency [2], [3]. Nevertheless, symbol detection in MU-MIMO systems is still a fundamental challenge, stemming from severe inter-user interference, which complicates the reliable recovery of transmitted symbols.

Past decades have witnessed persistent efforts in addressing MU-MIMO detection, including the classical model-based and the recently emerged neural detection approaches. Classical

model-based detectors—such as maximum-likelihood (ML) detection and maximum a-posteriori (MAP) estimation—offer optimal symbol recovery but require exhaustive evaluation of all symbol combinations, leading to exponential complexity with respect to system dimension [4]. To reduce complexity, suboptimal alternatives such as symbol-wise detection simply treat interference as noise, yet inevitably sacrificing detection accuracy and throughput [5]. These limitations have motivated the development of iterative interference cancellation schemes [6], which refine soft symbol estimates across iterations using probabilistic reasoning. Such methods can closely approach MAP performance with only polynomial complexity by iteratively canceling estimated interference [7], especially when enhanced with soft decoding [8]–[10]. However, their performance can degrade substantially in scenarios with imperfect Channel State Information (CSI) or when the channel deviates from the linear Gaussian model.

To overcome these limitations, deep learning (DL)-based detectors have attracted increasing attention for MU-MIMO symbol detection. In particular, model-driven DL architectures based on deep unfolding have demonstrated remarkable performance gains by embedding domain knowledge from classical detectors into trainable neural networks (see [11], [12] and references therein). Representative works include OAMP-Net2 [13], which unfolds the orthogonal approximate message passing (OAMP) detector [14] with a small number of trainable parameters to enhance robustness under channel uncertainty; MMNet [15], which is inspired by iterative soft-thresholding algorithms and exploits temporal and spectral correlations in realistic channels to accelerate training; GEP-Net [16], [17], which incorporates Graph Neural Networks (GNNs) into the expectation propagation (EP) framework [18] to improve message passing at the cost of increased computational complexity; and AMP-GNN [19], which further reduces complexity by unfolding the Approximate Message Passing (AMP) algorithm [20] with embedded GNN modules, achieving a favorable trade-off between complexity and Symbol Error Rate (SER). Despite their effectiveness, model-driven architectures remain fundamentally constrained by the assumptions and limitations of the underlying algorithms, which makes the generalization with respect to different system and user configurations challenging.

These limitations have motivated the development of *data-driven* neural detectors. Representative works include the early DNN-based approach DetNet [21], which unfolds a projected gradient descent algorithm for MIMO detection and demonstrates improved robustness compared to classical AMP

The authors are with the School of Information Science and Engineering, Southeast University, Nanjing 210096, China. Emails: {yongweiyi, xyi, wangwj, li_xiao, jinshi}@seu.edu.cn.

Part of this work has been presented at the IEEE ICC 2025 [1].

under certain channel conditions, but typically requires a large amount of training data and suffers performance degradation at higher modulation orders; ViterbiNet [22], which replaces the classical Viterbi algorithm with a simplified DNN for detection over finite-memory channels, but suffers from poor scalability with channel memory length; RE-MIMO [23], which further exploits recurrent and permutation-equivariant architectures to unfold classical iterative detectors, achieving improved performance through attention-based message passing at the cost of increased model complexity and training difficulty; ChannelNet [24], which exploits architectural symmetry through channel embedding and antenna-wise parameter sharing to reduce complexity, yet typically requires a large number of iterations to achieve high detection accuracy; and more recently SGT [25], which introduces a graph-based transformer architecture to enhance message passing in iterative detection, but entails substantial computational overhead and training cost due to its large-scale attention modules.

Of particular relevance to the current work is DeepSIC [26], which provides a representative neural realization of Soft Interference Cancellation (SIC) by replacing both the interference cancellation and soft decoding stages with trainable neural modules. DeepSIC infers soft symbol estimates from the received signals without relying on explicit probabilistic modeling, while preserving the iterative structure of classical SIC. Subsequent extensions of DeepSIC have investigated its robustness and adaptability under more challenging channel conditions, including meta-learning based schemes for handling rapidly varying channels [27] and hypernetwork-based architectures for scalable and adaptive MIMO detection [28]. As reported in prior work, DeepSIC and its extensions achieve competitive detection performance across a wide range of MIMO configurations, making them widely adopted baselines for learning-based multiuser detection.

Despite excellent empirical performance, the success of DeepSIC naturally raises questions regarding the model expressivity and generalization performance. For the former, is the size of neural networks sufficient to mimic the iterative SIC? For the latter, how many training samples are sufficient to train a model that is generalizable to different network and user configurations? With respect to the model expressivity, DeepSIC assigns independent neural modules to each user and each SIC iteration, which causes the number of trainable parameters to grow rapidly with the system dimension and iteration depth. Although this design does not prevent strong empirical performance in moderate-sized settings, it may limit sample efficiency and generalizability when applied to larger or deeper SIC architectures. With respect to the model generalization, the majority of existing works verify the models through extensive experiments, while there is still a lack of theoretical generalization analysis.

Generalization analysis aims to provide theoretical guarantees for learning algorithms with respect to data distributions, network architectures, model parameters, and training algorithms. This line of research has recently attracted increasing attention in the wireless communication community. Existing works have primarily focused on the learning of decoders or codebooks under fixed channel models or additive noise

assumptions, establishing generalization bounds for decoder selection, codebook design, and related surrogate losses [29], [30]. More recently, generalization analyses using Rademacher complexity have been developed for neural belief propagation decoders operating on Tanner graphs, explicitly characterizing the impact of code parameters, graph connectivity, and iteration depth [31]. Of particular relevance is the generalization analysis in [32] for deep learning-based MIMO detectors, showing that data-driven ReLU networks can asymptotically approximate the MAP detector, with generalization error controlled by the training sample size.

While these results provide important insights into the learnability of decoder architectures in coded communication systems and deep MIMO detectors, they share a common underlying assumption that the computation graph or functional structure is fixed *a priori* or independent of the physical channel realization. In contrast, neural receivers for multi-user detection operate on interference graphs induced by the physical channel itself, and rely on user-level message passing for soft interference mitigation. The resulting channel-induced interaction patterns, together with iterative neural processing across multiple users and iterations, lead to a hierarchical computation structure that is not explicitly captured by existing theoretical frameworks. Although generalization analyses for deep MIMO detectors have been reported in [32], such results typically treat the neural receiver as a black-box function class and provide limited insight into how architectural choices affect the generalization behavior of practical neural multi-user receivers. These limitations call for a new analytical framework for generalization analysis that takes both network architecture and model parameters into account.

Motivated by these considerations, we propose to inspect the DeepSIC-type MU-MIMO detection from a new architectural perspective as a Network-of-Multi-Layer Perceptrons (MLPs), which is composed of a number of MLPs interconnected by outer and inner Directed Acyclic Graphs (DAGs). Within such a network architecture, DeepSIC can be seen as a special case, for which it can be further upgraded as a more compact network architecture with substantially reduced model parameters. The generalization analysis is also conducted for such a *Network-of-MLPs*, revealing how network architectures and model parameters play a role in the required number of training samples for generalization. The main contributions of this work are summarized as follows:

- Within the architecture of *Network-of-MLPs*, we propose *GNNSIC*, a data-driven soft interference cancellation framework for MU-MIMO detection. The proposed method formulates the iterative SIC procedure as a graph-based message-passing process and employs GNN modules to perform interference cancellation and soft symbol detection. By imposing parameter sharing across users and SIC iterations, GNNSIC achieves a compact architecture with substantially fewer trainable parameters than DeepSIC. The extensive simulation results demonstrate that GNNSIC attains comparable or improved SER performance to DeepSIC in various linear/nonlinear channels with/without CSI uncertainty and possesses excellent user generalization performance, with significantly fewer

parameters and training samples.

- We formulate a novel framework of norm-based generalization analysis for the *Network-of-MLPs* architecture with Rademacher complexity, relating generalization performance to the network architectures and Frobenius norms of the model parameters. The proposed *Network-of-MLPs* consists of an outer DAG that captures the SIC iteration structure and inner DAGs that represent the MLP computations within each block. We develop a two-level peeling-based analysis that separately controls the inner and outer DAGs, enabling a compositional characterization of the overall Rademacher complexity. Such analyses have proven effective for deep architectures with compositional structures and parameter sharing, making them well-suited for studying learning-based iterative multi-user receivers with soft interference mitigation and shared neural components.
- Under the analytical generalization framework, we derive corresponding norm-based generalization bounds for both DeepSIC and GNNSIC. For DeepSIC, the absence of parameter sharing across iterations leads to a multiplicative accumulation of block-wise operator norms, while the unrolled outer DAG structure introduces degree-dependent amplification through repeated peeling, which together yield an exponential dependence of the complexity on the SIC depth. In contrast, for GNNSIC, extensive parameter sharing across both network blocks and outer iterations collapses the outer DAG to a single shared layer, thereby preventing both norm accumulation and degree amplification and yielding a substantially tighter bound independent of the SIC depth. This provides a theoretical explanation for the improved generalization behavior of GNNSIC observed in the numerical results.

The rest of this paper is organized as follows. Section II introduces the system model and reviews iterative SIC and DeepSIC. Section III formalizes the *Network-of-MLPs* abstraction and shows how DeepSIC fits into this framework. Section IV presents the proposed GNNSIC architecture. Section V develops the generalization analysis for DeepSIC and GNNSIC. Section VI reports the experimental results, and Section VII concludes the paper.

II. SYSTEM MODEL, ITERATIVE SIC AND DEEPSIC

A. System Model

We consider an uplink multiuser communication system in which multiple single-antenna users simultaneously transmit their data over the same frequency resource to a multi-antenna base station. In this work, the communication system is modeled as symbol transmission over a linear channel characterized by the channel matrix \mathbf{H} , impaired by additive white Gaussian noise (AWGN), i.e.,

$$\mathbf{y} = \mathbf{H}\mathbf{s} + \mathbf{w}, \quad (1)$$

where $\mathbf{y} \in \mathbb{R}^N$ is the channel output, representing the received signal at the base station. $\mathbf{H} = [\mathbf{h}_1, \mathbf{h}_2, \dots, \mathbf{h}_K] \in \mathbb{R}^{N \times K}$ is the channel matrix, where \mathbf{h}_i is the user- i 's channel, encapsulating the channel coefficients between the i -th user

and the N receiver antennas at the base station. The users' channels are assumed to be constant during communication and known to the receiver. $\mathbf{s} = (s_1, s_2, \dots, s_K) \in \mathcal{M}^K$ represents the input symbols transmitted by the K users. Each element of \mathbf{s} is drawn from a constellation set \mathcal{M} with size M , where M denotes the number of constellation points (e.g., for BPSK, $M = 2$), and $\mathbf{w} \in \mathbb{R}^N$ is an independent multivariate Gaussian noise vector with zero mean and covariance $\sigma_n^2 \mathbf{I}_N$.

Different from the most popular line of research that is dedicated to model-based/driven MIMO detection, we place our focus on the iterative SIC and its data-driven counterpart.

B. Iterative SIC

The iterative SIC algorithm [8] is to enhance multiuser detection by iteratively canceling interference across multiple stages and making soft decisions. In each iteration, the conditional distribution of the input symbol for a given user, s_i , is estimated based on the channel output \mathbf{y} , by utilizing previous estimates of the conditional distributions of the interfering symbols. By recursively applying this process, the estimates of the conditional distributions are progressively refined, so that the final detection of the input symbols is obtained based on the conditional distributions in the final iteration.

The iterative SIC algorithm involves L iterations, each consisting of two main steps performed in parallel: interference cancellation and soft detection.

- 1) **Interference Cancellation:** For the i -th user and the l -th iteration, interference cancellation starts by estimating the interference from other users $k \neq i$. The interference generated by other users can be collected as $\{\mathbf{h}_k s_k\}_{k \neq i}$. Since s_k cannot be directly observed by the receiver, an estimate at the previous iteration, $\hat{s}_k^{(l-1)}$, can be obtained through its expected value $\mathbb{E}[\hat{s}_k^{(l-1)}]$, where $\hat{s}_k^{(l-1)}$ takes all possible constellation points in \mathcal{S} with the probabilities provided by the previous iteration $\hat{\mathbf{p}}_k^{(l-1)}$, and the variance $\text{Var}(\hat{s}_k^{(l-1)})$. Therefore, the interference from other users can be subtracted from the received channel output \mathbf{y} , where the symbols $\{s_k\}_{k \neq i}$ are replaced by their expected estimate, i.e., $\{\mathbb{E}[\hat{s}_k^{(l-1)}]\}_{k \neq i}$.
- 2) **Soft Detection:** In the soft detection step, the input symbols for user i at iteration l are estimated based on the conditional distribution $\hat{\mathbf{p}}_i^{(l)}$. Let $\mathbf{z}_i^{(l)} \in \mathbb{R}^N$ represent the updated channel output after interference cancellation, which is given by

$$\mathbf{z}_i^{(l)} = \mathbf{h}_i s_i + \sum_{k \neq i} \mathbf{h}_k \Delta s_k^{(l-1)} + \mathbf{w}, \quad (2)$$

where $\Delta s_k^{(l-1)}$ denotes the residual estimation error of the interfering symbol s_k at iteration $(l-1)$, defined as $\Delta s_k^{(l-1)} = s_k - \mathbb{E}[\hat{s}_k^{(l-1)}]$. Thus, the conditional distribution of $\mathbf{z}_i^{(l)}$, given the input symbol s_i set to a constellation point $\alpha_m \in \mathcal{M}$, corresponds to a multivariate Gaussian distribution with mean value $\mathbf{h}_i \alpha_m$ and covariance $\sum_{k \neq i} \mathbf{h}_k \mathbf{h}_k^T \text{Var}(\hat{s}_k^{(l-1)}) + \sigma_n^2 \mathbf{I}_N$. For each constellation point α_m , the estimated conditional distribution $\hat{\mathbf{p}}_i^{(l)}$ is approximated using Bayes' theorem.

After the final iteration, the detected symbol is the one that maximizes the conditional distribution $\hat{\mathbf{p}}_i^{(L)}$ for each user, i.e., $\hat{s}_i = \alpha_{m^*}$ where $m^* = \arg \max_{m \in \{1, \dots, M\}} \left(\hat{\mathbf{p}}_{i,m}^{(L)} \right)$.

C. DeepSIC

DeepSIC [26] is a data-driven implementation based on the iterative SIC algorithm. This method utilizes a series of interconnected neural network blocks to perform both the interference cancellation and soft detection stages inherent in the iterative SIC process. By transforming these sequential stages into a classification task, DeepSIC leverages the power of neural networks to enhance performance and robustness in complex signal environments.

Each network block in DeepSIC corresponds to a specific user and iteration. For the i -th user at the l -th iteration, the estimated conditional distribution $\hat{\mathbf{p}}_i^{(l)}$ for symbol s_i is computed based on the realization of the channel output \mathbf{y} and the conditional distribution estimates obtained from the previous iteration for other users. This classification task is implemented using fully connected neural networks with a softmax layer, where the input features are the channel output, and the training label is the input symbol s_i for user i .

DeepSIC's architecture consists of multiple network blocks working in tandem. Specifically, each building block performs both interference cancellation and soft decoding for a given user. The output of each block is the estimated conditional probabilities of input symbols, denoted as $\hat{\mathbf{p}}_i^{(l)}$ for user i at iteration l . For a system with K users and L iterations, DeepSIC is constructed with $K \times L$ network blocks, providing comprehensive and iterative predictions of the input symbols.

The neural network blocks are trained using supervised learning. The training data consists of pairs of input features and corresponding transmitted symbols. The network is trained to minimize the cross-entropy loss between the predicted and actual symbol distributions. This training process enables the network to learn to accurately predict the conditional probabilities of the transmitted symbols.

Compared to the iterative SIC, DeepSIC promises excellent detection performance for both linear and non-linear channels as well as enhanced robustness to CSI uncertainty. However, DeepSIC requires a large number of received signal samples to train and retrain the models when the number of users varies. This is the motivation of our current work.

III. NETWORK-OF-MLPS

In what follows, we reformulate DeepSIC in a general *Network-of-MLPs* manner, which facilitates a new network architecture design in Section IV and generalization analysis in Section V.

A. Network-of-MLPs: Architecture and Notation

Notations: Throughout the paper, expressions of the form $(x_\mu)_{\mu=1}^b$ denote an ordered collection (i.e., a tuple or sequence) indexed by μ , rather than an unordered set.

We introduce a unified architecture, referred to as a *Network-of-MLPs*, which serves as a common representation

for a broad class of iterative neural detectors. The outer architecture is represented by a directed acyclic graph (DAG) $G^{(\text{out})} = (\mathcal{V}^{(\text{out})}, \mathcal{E}^{(\text{out})})$, whose nodes correspond to multiple *network blocks*. We index the network blocks by user $k \in [K] \triangleq \{1, \dots, K\}$ and outer iterations by $l \in [L]$. Each network block is itself a Multilayer Perceptron (MLP) and therefore induces an inner DAG. Each inner MLP block \mathcal{B}_{k_l} is associated with a directed acyclic graph $G_{k_l}^{(\text{in})} = (\mathcal{V}_{k_l}^{(\text{in})}, \mathcal{E}_{k_l}^{(\text{in})})$ composed of $N + 1$ layers indexed by $n = 0, \dots, N$, where $n = 0$ corresponds to the input layer. From this perspective, the overall model can be viewed as a *DAG-of-DAGs*, where each MLP block is a super-node in the outer graph.

The architecture is organized hierarchically, with an outer structure indexed by network block k and iteration l , and an inner MLP structure of depth N within each block. Each block processes local input features and produces an intermediate soft estimate. The j -th neuron in layer n is denoted by $\mathbf{z}_{k_l,j}^{(\text{in}),n}$,

and we write $\mathbf{v}_{k_l}^{(\text{in}),n} = (\mathbf{z}_{k_l,j}^{(\text{in}),n})_{j=1}^{q_{k_l,n}^{(\text{in})}}$ for the collection of neurons in that layer. The width of layer n is $q_{k_l,n}^{(\text{in})}$, and c_n denotes the number of channels at that layer. Computation in \mathcal{B}_{k_l} is parameterized by layer-wise weight matrices $\mathbf{W}_{k_l}^{(\text{in}),1}, \dots, \mathbf{W}_{k_l}^{(\text{in}),N}$. For $1 \leq n \leq N - 1$, $\mathbf{W}_{k_l,j}^{(\text{in}),n}$ is the weight matrix associated with the j -th neuron in layer n and maps the concatenated activations of its predecessor neurons to \mathbb{R}^{c_n} . The final matrix $\mathbf{W}_{k_l}^{(\text{in}),N} \in \mathbb{R}^{M \times q_{k_l,N}^{(\text{in})}}$ implements a linear readout producing an M -dimensional output. For any neuron $\mathbf{z}_{k_l,j}^{(\text{in}),n}$, $\text{pred}(n, j)_{k_l}$ denotes the set of neurons in layer $n - 1$ connected to it by directed edges in \mathcal{E}_{k_l} . For a fixed outer iteration l , the layer-wise sparsity of the inner DAG for block \mathcal{B}_{k_l} is defined as $d_{k_l,n}^{(\text{in})} \triangleq \max_{j \in [q_{k_l,n}^{(\text{in})}]} |\text{pred}(n, j)_{k_l}|$, and the maximum inner sparsity

at outer iteration l is given by $d_{l,n}^{(\text{in})} \triangleq \max_{k \in [K]} d_{k_l,n}^{(\text{in})}$. Dependencies across blocks are realized through structured interconnections—such as feature concatenation or aggregation—which encode the algorithmic interactions across network blocks and iterations. At outer layer l , the collection of network blocks is denoted by $\mathbf{v}^{(\text{out}),l} = (\mathbf{z}_{k_l}^{(\text{out}),l})_{k_l=1}^{q_l^{(\text{out})}}$, where

$q_l^{(\text{out})}$ is the width of that layer and $\mathbf{z}_{k_l}^{(\text{out}),l}$ denotes the k_l -th block. Each block produces a vector-valued representation in \mathbb{R}^{c_l} , where c_l denotes the number of channels at outer iteration l . The transformations across outer layers are parameterized by weight matrices $\mathbf{W}^{(\text{out}),1}, \dots, \mathbf{W}^{(\text{out}),L}$, where $\mathbf{W}_{k_l}^{(\text{out}),l} \in \mathbb{R}^{c_l \times (c_{l-1} \cdot |\text{pred}(l, k_l)|)}$ aggregates the representations from the predecessor blocks in layer $l - 1$ according to the connectivity pattern defined by $\mathcal{E}^{(\text{out})}$. For a block $\mathbf{z}_{k_l}^{(\text{out}),l}$, we denote by $\text{pred}(l, k_l)$ the set of its predecessor blocks in the $(l - 1)$ -th outer layer. The layer-wise sparsity of the outer DAG is quantified by the maximum in-degree $d_l^{(\text{out})} \triangleq \max_{k_l \in [q_l^{(\text{out})}]} |\text{pred}(l, k_l)|$.

Global degree parameters: To characterize the overall sparsity of the *Network-of-MLPs*, we define

$$\bar{d}^{(\text{out})} \triangleq \max_{l \in [L]} d_l^{(\text{out})}, \quad \bar{d}^{(\text{in})} \triangleq \max_{l \in [L], n \in [N-1]} d_{l,n}^{(\text{in})}.$$

These quantities serve as global descriptors of the outer- and inner-level DAG sparsity and will be used to express the final

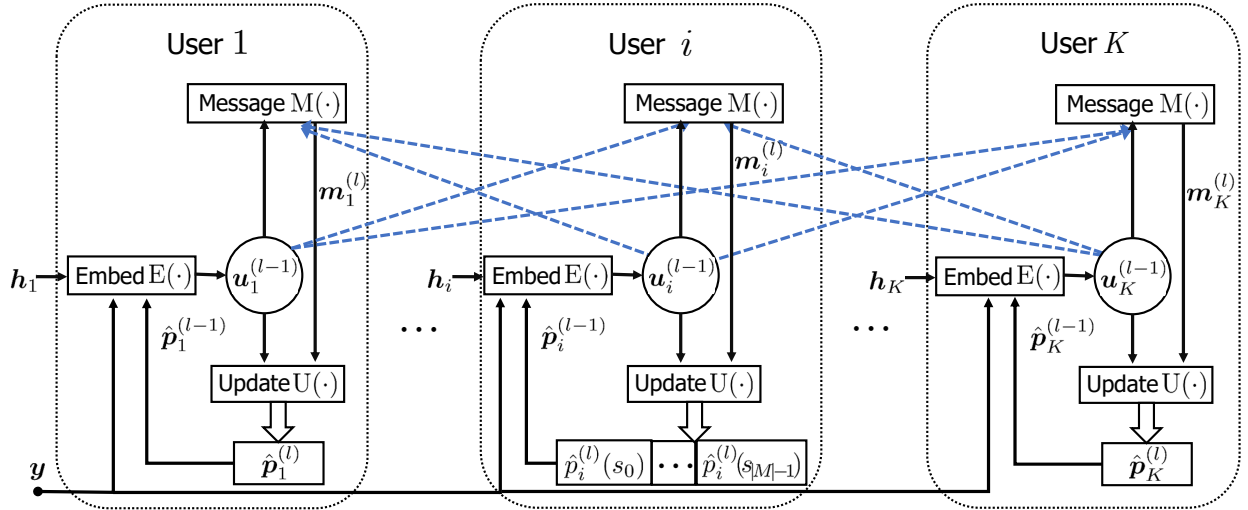


Fig. 1: The internal structure of a GNNSIC network block at the l -th iteration. Each user node forms its block input by concatenating the received signal \mathbf{y} , the channel state h_i , and the prior soft symbol estimate $\hat{\mathbf{p}}_i^{(l-1)}$, which are processed by a set of MLPs constituting the inner computation graph. Blue dashed lines indicate message exchanges among user nodes induced by the underlying interference graph. This block is repeatedly applied across iterations according to the outer DAG defined by the *Network-of-MLPs* architecture.

complexity bounds.

Input energy assumption: Assume there exists a constant $E_0 > 0$ such that

$$\max_{k_0} \sum_{t=1}^T \left\| z_{k_0}^{(\text{out}),0}(\mathbf{x}_t) \right\|_2^2 \leq E_0.$$

Formally, the architecture comprises K network blocks unrolled over L outer iterations, resulting in a total of $K \times L$ MLP blocks and inducing a DAG-of-DAGs computation graph. This abstraction separates the local nonlinear transformations within individual MLPs from the global information propagation across network blocks and iterations. Both DeepSIC and GNNSIC can be interpreted as specific instantiations of this framework through different choices of block connectivity and parameter sharing, which enables a unified analysis of model complexity and generalization behavior in subsequent sections.

B. DeepSIC as Network-of-MLPs

DeepSIC [26] can be naturally interpreted as a specific instantiation of the proposed *Network-of-MLPs* architecture, obtained by unrolling the classical iterative SIC algorithm and replacing its analytical processing steps with learned neural modules.

In DeepSIC, each *network block* corresponds to a particular user and a particular SIC iteration. For the i -th user at iteration l , the associated MLP block produces an estimate of the conditional symbol distribution $\hat{\mathbf{p}}_i^{(l)}$ based on the received signal \mathbf{y} and the soft symbol estimates of the remaining users from the previous iteration. Within the *Network-of-MLPs* abstraction, this corresponds to an outer DAG in which blocks at iteration l receive inputs from multiple blocks at iteration $l-1$ through feature concatenation.

Each block is implemented as a fully connected MLP with a softmax output layer, thereby realizing a local classification

task. The input features consist of the channel observation together with the concatenated soft estimates from other users, while the training label is the transmitted symbol s_i of the corresponding user. For a system with K users and L SIC iterations, the resulting architecture contains $K \times L$ MLP blocks, with no parameter sharing across users or iterations.

From a structural perspective, DeepSIC therefore corresponds to a *Network-of-MLPs* with dense inter-block connectivity induced by feature concatenation and with independently parameterized blocks. While this design offers strong empirical performance for both linear and nonlinear channels, it also leads to a hypothesis space whose complexity grows rapidly with the number of users and iterations. As will be analyzed in Section V, this lack of parameter sharing plays a central role in the generalization behavior of DeepSIC and motivates the structured and shared architecture adopted by GNNSIC.

IV. GNNSIC FRAMEWORK

This section presents GNNSIC, a graph-based neural MIMO detection framework that can be interpreted as a structured instantiation of the *Network-of-MLPs* architecture introduced earlier. Similar to DeepSIC, GNNSIC follows the iterative SIC paradigm while employing learnable nonlinear processing. Unlike DeepSIC, GNNSIC explicitly models inter-user interference through a conflict graph, which induces a structured outer DAG over a collection of neural network blocks. This topology-aware design enables efficient representation of inter-user dependencies and facilitates extensive parameter sharing across users and iterations, resulting in a substantially reduced model complexity.

A. Overview of GNNSIC

From the *Network-of-MLPs* perspective, GNNSIC can be viewed as a collection of network blocks organized over

an outer DAG indexed by users and iterations. Each block implements a fixed inner computation graph, realized by a set of MLPs that perform local nonlinear processing and themselves form a DAG. The outer DAG then specifies how the outputs of these inner graphs are propagated across blocks through explicit feature concatenation.

1) *Topology-aware Modeling of Multiuser Interference:* GNNSIC represents multiuser interference using a fully connected, bidirectional graph $\mathcal{G}^{(\text{phy})} = (\mathcal{V}^{(\text{phy})}, \mathcal{E}^{(\text{phy})})$, where each node $v_i^{(\text{phy})} \in \mathcal{V}^{(\text{phy})}$ corresponds to a user, and each directed edge $(v_i^{(\text{phy})}, v_j^{(\text{phy})}) \in \mathcal{E}^{(\text{phy})}$ encodes the interference from user i to user j . Within the *Network-of-MLPs* abstraction, each GNN iteration corresponds to one application of a shared network block, while the graph structure specifies the outer-DAG connectivity among blocks.

A shared GNN module is iteratively applied over L iterations to refine the symbol estimates. The structure of the l -th iteration is depicted in Fig. 1. All iterations share an identical set of parameters, such that the iterative procedure can be interpreted as an unrolling of the same network block over the outer DAG, rather than a stack of independent layers. Accordingly, each iteration corresponds to one unfolding of the outer DAG in terms of information flow, while not increasing the model capacity. Information is propagated across iterations by directly concatenating the current soft symbol estimates with the received signal and channel features. The complete GNNSIC procedure is summarized in Algorithm 1.

2) *Parameter Sharing Strategies:* Within the *Network-of-MLPs* framework, the key architectural novelty of GNNSIC lies in its extensive parameter sharing across both the iteration and user dimensions, which significantly enhances model compactness and generalizability.

Cross-Iteration Sharing: All network blocks across iterations share an identical set of parameters. Specifically, the MLPs used for node embedding, message generation, and symbol update are reused at every iteration. This recursive application of a single shared block corresponds to repeatedly traversing the outer DAG, with intermediate representations from the previous iteration concatenated into the input of the next block. Such a design decouples the number of inference iterations from the model capacity: although the block is unrolled for L iterations during inference, the effective depth of the hypothesis class is determined by a single shared network block.

Cross-User Sharing: Within each iteration, all user nodes employ the same embedding, message, and update functions. From the *Network-of-MLPs* viewpoint, this implies that all network blocks associated with different users are parameter-tied, differing only in their local input features. This user-agnostic design enables GNNSIC to generalize across varying numbers of users without retraining, while preserving a consistent outer-DAG structure. Importantly, such parameter tying prevents the effective model capacity from scaling with the number of users, a property that will be formally reflected in the generalization analysis.

Through both cross-iteration and cross-user parameter sharing, GNNSIC realizes a highly compact *Network-of-MLPs*

Algorithm 1 GNNSIC

Input: Channel output \mathbf{y} ; channel matrix \mathbf{H} ; noise variance σ_w^2 .

Initialization:

- Define the graph $\mathcal{G}^{(\text{phy})} = (\mathcal{V}^{(\text{phy})}, \mathcal{E}^{(\text{phy})})$, where $\mathcal{V}^{(\text{phy})}$ denotes the set of users (nodes) and $\mathcal{E}^{(\text{phy})}$ the set of edges.
- Initialize the symbol posterior of each node $i \in \mathcal{V}^{(\text{phy})}$ as

$$\hat{\mathbf{p}}_i^{(0)} = \frac{1}{M} \mathbf{1} \in \mathbb{R}^M.$$

Main Procedure:

- 1: **for** $l = 1, \dots, L$ **do**
- 2: $\mathbf{u}_i^{(l-1)} \leftarrow \mathbb{E}(\mathbf{y}, \mathbf{h}_i, \hat{\mathbf{p}}_i^{(l-1)})$
- 3: **for** $i \in \mathcal{V}$ **do**
- 4: $\mathbf{m}_i^{(l)} \leftarrow \text{mean}(\{\mathbb{M}(\mathbf{u}_i^{(l-1)}, \mathbf{u}_k^{(l-1)}, \mathbf{e}_{ik}^{(l-1)}) \mid k \in \mathcal{N}(i)\})$
- 5: $\hat{\mathbf{p}}_i^{(l)} \leftarrow \text{U}(\mathbf{u}_i^{(l-1)}, \mathbf{m}_i^{(l)})$
- 6: **end for**
- 7: **end for**

Output: Final symbol estimate via hard decision:

$$m_i^* = \arg \max_{m \in \{1, \dots, M\}} \hat{\mathbf{p}}_{i,m}^{(L)}, \quad \forall i \in \mathcal{V}. \quad (7)$$

architecture, achieving reduced model complexity and memory usage while retaining strong expressive power.

B. GNNSIC for MIMO Detection

1) *Initialization of Symbol Estimates:* At the beginning of the detection process, the initial soft estimate for each user i is set to a uniform distribution over the modulation alphabet, i.e., $\hat{\mathbf{p}}_i^{(0)} = \frac{1}{M} \cdot \mathbf{1} \in \mathbb{R}^M$, where M denotes the modulation order and $\mathbf{1}$ is an all-one vector, assuming equal probability for all symbols in the constellation \mathcal{M}^M .

2) *GNN Module at Iteration l :* Each GNN module, corresponding to a single network block in the proposed *Network-of-MLPs* framework, consists of three stages: node feature embedding, message passing, and symbol estimate updating.

a) *Node Feature Embedding:* At the beginning of the l -th iteration, each user node i constructs its input feature vector by concatenating the received signal \mathbf{y} , the channel vector \mathbf{h}_i , and the soft symbol estimate from the previous iteration $\hat{\mathbf{p}}_i^{(l-1)}$. This concatenated vector is then transformed into a higher-dimensional latent representation via a shared embedding function:

$$\mathbf{u}_i^{(l-1)} = \mathbb{E}(\mathbf{y}, \mathbf{h}_i, \hat{\mathbf{p}}_i^{(l-1)}), \quad (3)$$

where $\mathbb{E} : \mathbb{R}^{2N+M} \rightarrow \mathbb{R}^{2a}$ denotes an MLP shared across users and iterations with a being the latent dimensionality.

b) *Message Passing:* Each node aggregates messages from its neighbors as follows:

$$\mathbf{m}_i^{(l)} = \text{mean}(\{\mathbb{M}(\mathbf{u}_i^{(l-1)}, \mathbf{u}_k^{(l-1)}, \mathbf{e}_{ik}^{(l-1)}) \mid k \in \mathcal{N}(i)\}), \quad (4)$$

where $M(\cdot)$ is a message generation function with a shared MLP across users and iterations followed by a softmax activation, and $e_{ik}^{(l-1)}$ denotes the edge feature between users i and k . The generated messages from user i 's neighbors, i.e., for all $k \in \mathcal{N}(i)$, are aggregated at user i with a $\text{mean}(\cdot)$ function, and then passed back to each neighbor $k \in \mathcal{N}(i)$.

c) *Symbol Estimate Updating*: Each user i then updates its symbol-wise posterior estimate according to the passed messages and its node feature embedding, i.e.,

$$\hat{\mathbf{p}}_i^{(l)} = \text{U} \left(\mathbf{u}_i^{(l-1)}, \mathbf{m}_i^{(l)} \right), \quad (5)$$

where $\text{U} : \mathbb{R}^{2a+M} \rightarrow \mathbb{R}^M$ is a shared MLP across users and iterations with a softmax output, yielding the refined symbol probability distribution for the next iteration.

3) *End-to-End Training and Loss Function*: Let the training dataset be denoted by $\{(\tilde{\mathbf{y}}_t, \tilde{\mathbf{s}}_t)\}_{t=1}^T$, where $\tilde{\mathbf{y}}_t$ represents the received signal vector and $\tilde{\mathbf{s}}_t$ denotes the corresponding transmitted symbol vector for the t -th training sample. GNNSIC is trained by minimizing the average cross-entropy loss over all users:

$$\mathcal{L}(\boldsymbol{\theta}) = \frac{1}{TK} \sum_{t=1}^T \sum_{i=1}^K -\log \left(\hat{\mathbf{p}}_i^{(L)}(\tilde{\mathbf{y}}_t, \tilde{\mathbf{h}}_{i,t}; \boldsymbol{\theta})_{\tilde{\mathbf{s}}_{i,t}} \right), \quad (6)$$

where $\boldsymbol{\theta}$ denotes the collection of all model parameters. Here, the iteration index l refers to repeated unrolling of the same parameter-shared network block over the outer DAG. This property will play a key role in the subsequent generalization analysis. The model is trained end-to-end using the Adam optimizer.

4) *Final Symbol Decision*: Upon completing the final iteration, the symbol detection for user i is given by $\hat{s}_i = \alpha_{m^*} \in \mathcal{M}^M$ such that

$$m^* = \arg \max_{m \in \{1, 2, \dots, M\}} \hat{\mathbf{p}}_{i,m}^{(L)}. \quad (7)$$

This rule selects the most probable symbol from the estimated posterior distribution.

V. GENERALIZATION ANALYSIS

Generalization analysis provides theoretical insight into why learning models can reliably perform well on unseen data, where a substantial body of work [33]–[40] has established norm-based generalization bounds for deep neural networks. Motivated by these results, we develop a Rademacher complexity-based generalization analysis for the *Network-of-MLPs* function class that explicitly accounts for its underlying DAG structure, and specialize the resulting bounds to DeepSIC and GNNSIC as two structurally distinct instantiations. This framework provides a principled way to upper-bound the generalization gap, defined as the difference between the expected test error and the empirical training error, for multi-class classification models.

Rademacher complexity characterizes the richness of a hypothesis class by quantifying its ability to correlate with random noise. Concretely, it measures the extent to which functions in the class can fit random label assignments generated by independent Rademacher variables taking values in $\{\pm 1\}$.

A larger Rademacher complexity indicates a higher-capacity hypothesis class that can more easily adapt to random fluctuations, which is commonly associated with an increased risk of overfitting and a larger expected generalization gap [35], [41], [42].

Definition 1 (Empirical Rademacher Complexity). Let \mathcal{W} denote the parameter space of the *Network-of-MLPs* architecture, and let $\mathcal{F} \triangleq \{f_{\mathbf{w}} : \mathbf{w} \in \mathcal{W}\}$ denote the associated hypothesis class. Each $f_{\mathbf{w}} : \mathcal{X}^K \rightarrow \mathbb{R}^{K \times M}$ maps a joint K -block input to K output vectors, each of dimension M .

Given a sample set $\mathcal{S}_x = \{\mathbf{x}_t\}_{t=1}^T$ with $\mathbf{x}_t \in \mathcal{X}^K$, the empirical Rademacher complexity of \mathcal{F} is defined as

$$\mathcal{R}_{\mathcal{S}_x}(\mathcal{F}) := \frac{1}{T} \mathbb{E}_{\xi} \left[\sup_{\mathbf{w} \in \mathcal{W}} \left| \sum_{t=1}^T \sum_{k=1}^K \sum_{m=1}^M \xi_{k,t,m} f_{\mathbf{w}}(\mathbf{x}_t)_{k,m} \right| \right], \quad (8)$$

where $\xi_{k,t,m}$ are independent Rademacher variables taking values in $\{\pm 1\}$. This quantity measures the ability of \mathcal{F} to fit random noise on the finite sample set \mathcal{S}_x .

We consider a multi-block classification task defined by a distribution P over $(\mathbf{x}, \mathbf{s}) \in \mathcal{X}^K \times [M]^K$. For any $f_{\mathbf{w}} \in \mathcal{F}$, the expected classification error is

$$\text{err}_P(\mathbf{w}) := \frac{1}{K} \sum_{k=1}^K \mathbb{E}_{(\mathbf{x}, \mathbf{s}) \sim P} \mathbb{I} \left[\max_{m \neq s_k} f_{\mathbf{w}}(\mathbf{x})_{k,m} \geq f_{\mathbf{w}}(\mathbf{x})_{k,s_k} \right]$$

where $\mathbb{I}(\cdot)$ is the indicator function. Given independent and identically distributed (i.i.d.) training samples $\mathcal{S} = \{(\mathbf{x}_t, \mathbf{s}_t)\}_{t=1}^T$, the empirical γ -margin error is defined as

$$\text{err}_{\mathcal{S}}^{\gamma}(\mathbf{w}) := \frac{1}{T} \sum_{t=1}^T \sum_{k=1}^K \mathbb{I} \left[\max_{m \neq s_{kt}} f_{\mathbf{w}}(\mathbf{x}_t)_{k,m} + \gamma \geq f_{\mathbf{w}}(\mathbf{x}_t)_{k,s_{kt}} \right].$$

Lemma 1 ([43, Lemma 2.2]). *With probability at least $1 - \delta$ over the draw of \mathcal{S} , the following generalization error gap holds uniformly for all $f_{\mathbf{w}} \in \mathcal{F}$:*

$$\text{err}_P(\mathbf{w}) - \text{err}_{\mathcal{S}}^{\gamma}(\mathbf{w}) \leq \frac{2\sqrt{2}}{\gamma} \mathcal{R}_{\mathcal{S}_x}(\mathcal{F}) + 3\sqrt{\frac{\log(2/\delta)}{2T}}. \quad (9)$$

Lemma 1 reduces the generalization analysis to controlling the empirical Rademacher complexity of the hypothesis class \mathcal{F} .

A. Network Architecture Definitions

We consider a multi-user predictor consisting of K users interacting through L outer iterations. The model is composed of $K \times L$ network blocks: for each user $k \in [K]$ and each outer iteration $l \in [L]$, there exists a corresponding block \mathcal{B}_{k_l} .

Each block \mathcal{B}_{k_l} is an inner MLP represented by a DAG of depth N , i.e., a feedforward computation graph with directed edges and no cycles. At a fixed outer iteration l , the K inner blocks $(\mathcal{B}_{k_l})_{k=1}^K$ operate in parallel across users. Across outer iterations, these blocks are coupled through learnable outer weights, which induce an outer DAG of depth L governing inter-user information flow over iterations.

The resulting architecture thus forms a hierarchical *Network-of-MLPs*, obtained by composing inner DAGs through an outer DAG with structured interactions across the K network blocks.

Inner MLP block \mathcal{B}_{k_l} . Fix a user $k \in [K]$ and an outer iteration $l \in [L]$. Let $G_{k_l}^{(\text{in})} = (\mathcal{V}_{k_l}^{(\text{in})}, \mathcal{E}_{k_l}^{(\text{in})})$ denote the DAG associated with the inner block \mathcal{B}_{k_l} , consisting of $N + 1$ layers indexed by $n = 0, \dots, N$. Following the notation in Section III-A, we write $\mathbf{z}_{k_l,j}^{(\text{in}),n}$ for the j -th neuron in layer n and $\mathbf{v}_{k_l}^{(\text{in}),n}$ for the collection of neurons in that layer.

The input to \mathcal{B}_{k_l} is defined as

$$\mathbf{x}_{k_l} = (\mathbf{z}_{k_l,j}^{(\text{in}),0})_{j=1}^{q_0^{(\text{in})}}.$$

For inner layers $1 \leq n \leq N - 1$, the neuron activations follow the standard MLP recursion

$$\mathbf{z}_{k_l,j}^{(\text{in}),n}(\mathbf{x}_{k_l}) = \sigma\left(\mathbf{W}_{k_l,j}^{(\text{in}),n} \mathbf{v}_{k_l,j}^{(\text{in}),n-1}(\mathbf{x}_{k_l})\right),$$

where $\sigma(\cdot)$ denotes the ReLU activation function, $\mathbf{v}_{k_l,j}^{(\text{in}),n-1}$ is the concatenation of predecessor activations, and $\mathbf{W}_{k_l,j}^{(\text{in}),n} \in \mathbb{R}^{c_n \times (c_{n-1} \cdot |\text{pred}(n,j)_{k_l}|)}$ is the corresponding weight matrix.

The inner block \mathcal{B}_{k_l} produces an M -dimensional score vector through a final linear readout layer,

$$\mathbf{f}_{k_l}^{(\text{in})}(\mathbf{x}_{k_l}) := \mathbf{W}_{k_l}^{(\text{in}),N} \mathbf{z}_{k_l}^{(\text{in}),N-1}(\mathbf{x}_{k_l}) \in \mathbb{R}^M.$$

The sparsity of the inner block is characterized by the layer-wise in-degree of its associated DAG. Specifically, we quantify the inner connectivity at layer n by the sparsity degree $d_n^{(\text{in})}$ and its worst-case counterpart $\bar{d}_{l,n}^{(\text{in})}$, as defined in Section III-A.

Outer network (across L steps and K blocks). We consider the composition of K network blocks over L outer iterations. The resulting outer architecture is represented by a DAG $G^{(\text{out})} = (\mathcal{V}^{(\text{out})}, \mathcal{E}^{(\text{out})})$ with $L + 1$ layers indexed by $l = 0, \dots, L$. Following the notation in Section III-A, we denote by $\mathbf{z}_{k_l}^{(\text{out}),l}$ the k_l -th network block at outer layer l , and by $\mathbf{v}^{(\text{out}),l}$ the collection of network blocks at that layer.

The input to the outer network is defined as

$$\mathbf{x} = (\mathbf{z}_{k_0}^{(\text{out}),0})_{k=1}^{q_0^{(\text{out})}},$$

For outer layers $1 \leq l \leq L$, the block-wise activations follow the recursive form

$$\begin{aligned} \mathbf{z}_{k_l,j}^{(\text{in}),0} &= \sigma\left(\mathbf{W}_{k_l}^{(\text{out}),l} \mathbf{v}_{k_l}^{(\text{out}),l-1}(\mathbf{x})\right), \\ \mathbf{z}_{k_l}^{(\text{out}),l}(\mathbf{x}) &= \mathbf{f}_{k_l}^{(\text{in})}(\mathbf{x}_{k_l}), \end{aligned}$$

where $\sigma(\cdot)$ denotes the ReLU activation function, $\mathbf{v}_{k_l}^{(\text{out}),l-1}$ denotes the concatenation of predecessor block activations, and $\mathbf{W}_{k_l}^{(\text{out}),l}$ is the corresponding aggregation weight matrix.

The sparsity of the outer composition is quantified by the layer-wise maximum in-degree of the outer DAG, denoted by $d_l^{(\text{out})}$ (see Section III-A).

Inner product-norm (per block). We define the inner product-norm, based on a product of maximum Frobenius norms, as

$$\rho_{\text{inner}}(\mathbf{w}_{k_l}) := \|\mathbf{W}_{k_l}^{(\text{in}),N}\|_F \cdot \prod_{n=1}^{N-1} \max_{i \in [q_n^{(\text{in})}]} \|\mathbf{W}_{k_l,i}^{(\text{in}),n}\|_F, \quad (10)$$

and assume a uniform bound $\rho_{\text{inner}}(\mathbf{w}_{k_l}) \leq \bar{\rho}_{\text{inner}}$ holds for all $k \in [K]$ and $l \in [L]$ throughout the analysis.

Outer product-norm. We define the outer product-norm, based on a product of maximum Frobenius norms, as

$$\rho_{\text{outer}}(\mathbf{w}) := \|\mathbf{W}^{(\text{out}),L}\|_F \cdot \prod_{l=1}^{L-1} \max_{k_l \in [q_l^{(\text{out})}]} \|\mathbf{W}_{k_l}^{(\text{out}),l}\|_F,$$

and assume a uniform bound $\rho_{\text{outer}}(\mathbf{w}) \leq \bar{\rho}_{\text{outer}}$ holds for the outer composition throughout the analysis.

Constrained hypothesis class. Given fixed inner- and outer-level capacity bounds $\bar{\rho}_{\text{inner}} > 0$ and $\bar{\rho}_{\text{outer}} > 0$, we consider networks whose parameters satisfy

$$\rho_{\text{inner}}(\mathbf{w}_{k_l}) \leq \bar{\rho}_{\text{inner}}, \quad \forall k \in [K], l \in [L],$$

and

$$\rho_{\text{outer}}(\mathbf{w}) \leq \bar{\rho}_{\text{outer}}.$$

These constraints induce a network-level complexity measure $\rho(\mathbf{w}) := \Phi(\rho_{\text{inner}}(\mathbf{w}_{k_l}), \rho_{\text{outer}}(\mathbf{w}))$, where Φ is a non-decreasing function in each argument.

Let

$$G \triangleq (G^{(\text{out})}, \{G_{k,l}^{(\text{in})}\}_{k \in [K], l \in [L]})$$

denote the overall computational DAG-of-DAGs of the *Network-of-MLPs*. We define the constrained hypothesis class as

$$\mathcal{F}_{G,\rho} := \{f_{\mathbf{w}} \in \mathcal{F}_G : \rho(\mathbf{w}) \leq \rho\}. \quad (11)$$

The Rademacher complexity of the class $\mathcal{F}_{G,\rho}$, and the resulting generalization bounds, are obtained via a two-level peeling argument, consisting of an inner- L -level step that controls each block through $\bar{\rho}_{\text{inner}}$ and an outer-level step that captures the compositional dependence across blocks through $\bar{\rho}_{\text{outer}}$.

B. Peeling Lemma for Network-of-MLPs

The analysis relies on a standard peeling argument for one-layer neural networks, originally established in [43]. For completeness and to align with the notation used in this paper, we restate the lemma below.

Lemma 2 (Peeling Lemma [43, Lemma 3.4]). *For any fixed inputs $\{\mathbf{x}_t\}_{t=1}^T$, let σ be a 1-Lipschitz, positively homogeneous activation applied element-wise (e.g., ReLU). Consider a class of vector-valued functions*

$$\mathcal{F} \subset \{f = (f_1, \dots, f_q) \mid f_j : \mathbb{R}^a \rightarrow \mathbb{R}^p, j \in [q]\},$$

and let $g : \mathbb{R} \rightarrow [0, \infty)$ be any convex and monotonically increasing function. Then, for any radius $R > 0$, the following inequality holds:

$$\begin{aligned} \mathbb{E}_{\xi} \sup_{\substack{f \in \mathcal{F}, \\ \mathbf{W} : \|\mathbf{W}_j\|_F \leq R}} g\left(\sqrt{\sum_{j=1}^q \left\| \sum_{t=1}^T \xi_t \sigma(\mathbf{W}_j f_j(\mathbf{x}_t)) \right\|_2^2}\right) \\ \leq 2 \mathbb{E}_{\xi} \left[\sup_{\substack{f \in \mathcal{F}, \\ j \in [q]}} g\left(\sqrt{q} R \left\| \sum_{t=1}^T \xi_t f_j(\mathbf{x}_t) \right\|_2\right) \right], \quad (12) \end{aligned}$$

where the supremum on the left is taken over all weight matrices $\{\mathbf{W}_j\}_{j=1}^q$ satisfying $\|\mathbf{W}_j\|_F \leq R$.

Proof. See Appendix A. \square

C. Theoretical Analysis

We now establish an upper bound on the empirical Rademacher complexity of the constrained hypothesis class $\mathcal{F}_{G,\rho}$ associated with the *Network-of-MLPs* architecture.

Proposition 1. *For a fixed sample set $\mathcal{S}_x = \{\mathbf{x}_t\}_{t=1}^T \subset \mathcal{X}^K$, the following bound holds. Then, the empirical Rademacher complexity of $\mathcal{F}_{G,\rho}$ admits the following upper bound:*

$$\mathcal{R}_{\mathcal{S}_x}(\mathcal{F}_{G,\rho}) \leq \frac{K\bar{\rho}_{\text{inner}}^L \bar{\rho}_{\text{outer}}}{T} (1 + \sqrt{2A})\sqrt{B}, \quad (13)$$

where the quantities A and B are defined as

$$\begin{aligned} A &:= (N+1)L \log 2 + L \log M \\ &+ \sum_{l=1}^L \log d_l^{(\text{out})} + \sum_{l=1}^L \sum_{n=1}^{N-1} \log d_{l,n}^{(\text{in})}, \\ B &:= \max_{k_0, \dots, k_L} \prod_{l=1}^L |\text{pred}(l, k_l)| \max_{j_0, \dots, j_N} \prod_{l=1}^L \prod_{n=1}^{N-1} |\text{pred}(n, j_n)_{k_l}| \\ &\cdot \max_{k_0} \sum_{t=1}^T \|\mathbf{z}_{k_0}^{(\text{out}),0}(\mathbf{x}_t)\|_2^2. \end{aligned}$$

The maximization in B is taken over all indices corresponding to valid paths in the network, i.e., such that $j_{n-1} \in \text{pred}(n, j_n)_{k_l}$ for all n and l , and $k_{l-1} \in \text{pred}(l, k_l)$. Here, M denotes the output dimension.

Proof. See Appendix B. \square

Theorem 1. *Let $\mathcal{F}_{G,\rho}$ be the constrained hypothesis class defined in (11), with $\rho = \bar{\rho}_{\text{inner}}^L \bar{\rho}_{\text{outer}}$. Let P be a distribution over $\mathcal{X}^K \times [M]^K$, and let $\mathcal{S} = \{(\mathbf{x}_t, \mathbf{s}_t)\}_{t=1}^T$ be a dataset of T i.i.d. samples drawn from P . Then, for any margin parameter $\gamma > 0$, with probability at least $1 - \delta$ over the draw of \mathcal{S} , the following generalization bound holds uniformly for all $f_{\mathbf{w}} \in \mathcal{F}_{G,\rho}$:*

$$\begin{aligned} \text{err}_P(\mathbf{w}) - \text{err}_{\mathcal{S}}^\gamma(\mathbf{w}) &\leq \frac{2\sqrt{2} K (\rho + 1)}{\gamma T} (1 + \sqrt{2A})\sqrt{B} \\ &+ 3\sqrt{\frac{\log(2(\rho + 2)^2/\delta)}{2T}}, \quad (14) \end{aligned}$$

where A and B are the architecture- and data-dependent complexity terms defined in Proposition 1.

Proof. See Appendix C. \square

Corollary 1. *Consider the setting of Proposition 1 and Theorem 1. Assume further that the interaction between network blocks across iterations is implemented via feature concatenation, and that no additional learnable linear transformation is applied between blocks. Then, the induced outer operator has unit norm, and the network-level norm bound simplifies to*

$$\rho = \bar{\rho}_{\text{inner}}^L.$$

Comparison of the Generalization Bounds: We compare the theoretical generalization bounds of DeepSIC and GNNSIC to highlight the impact of parameter sharing.

DeepSIC: The DeepSIC architecture follows the standard *Network-of-MLPs* architecture which consists of K distinct neural network blocks unrolled over L iterations. The input feature vector for the k -th user at time index t , denoted as $\mathbf{x}_{t,k}^{\text{Deep}} \in \mathbb{R}^{N+(K-1)(M-1)}$, is constructed by concatenating the received signal $\mathbf{y}_t \in \mathbb{R}^N$ with the soft symbol estimates from the previous iteration $(l-1)$ for the remaining $K-1$ users, $(\hat{\mathbf{p}}_{t,i}^{(l-1)})_{i \neq k}$. Since the interaction between blocks is implemented solely via feature concatenation, Corollary 1 applies directly.

With the notation and assumptions in Section III-A, the Rademacher complexity of DeepSIC is governed by the auxiliary terms A_D and B_D , which admit the bounds

$$\begin{aligned} A_D &\leq L \log \left(2^{N+1} M \bar{d}^{(\text{out})} (\bar{d}^{(\text{in})})^{N-1} \right), \\ B_D &\leq (\bar{d}^{(\text{out})})^L (\bar{d}^{(\text{in})})^{L(N-1)} \cdot E_0. \end{aligned}$$

The resulting generalization gap is therefore bounded by

$$\tilde{\mathcal{O}} \left(\frac{K(\rho + 1)}{T} (\bar{d}^{(\text{out})})^{\frac{L}{2}} (\bar{d}^{(\text{in})})^{\frac{L(N-1)}{2}} \sqrt{LE_0} \right), \quad (15)$$

where $\rho = \bar{\rho}_{\text{inner}}^L$ follows from Corollary 1.

GNNSIC: GNNSIC can be viewed as a special case of the proposed *Network-of-MLPs* framework with a single outer layer ($L = 1$) and fully shared parameters. GNNSIC substantially reduces the hypothesis space complexity through two forms of parameter sharing: (i) *cross-user sharing*, whereby all users employ a single shared neural network block, and (ii) *cross-iteration sharing*, whereby the same parameters are reused across message-passing iterations. As a result, the depth-dependent complexity terms in the generalization bound effectively collapse to $L = 1$, and the corresponding degrees are independent of the outer iteration index. Moreover, due to cross-user sharing, the maximization over computation paths reduces to a single user index. The input feature $\mathbf{x}_{t,k}^{\text{GNN}} \in \mathbb{R}^{2N+M}$ consists of the received signal \mathbf{y}_t , the channel vector \mathbf{h}_{kt} , and the soft symbol estimate $\hat{\mathbf{p}}_{kt}^{(l-1)}$. Consequently, under the global notation introduced in Section III-A, the auxiliary complexity terms for GNNSIC can be expressed as

$$\begin{aligned} A_G &\leq \log \left(2^{N+1} M \bar{d}^{(\text{out})} (\bar{d}^{(\text{in})})^{N-1} \right), \\ B_G &\leq \bar{d}^{(\text{out})} (\bar{d}^{(\text{in})})^{N-1} \cdot E_0, \end{aligned}$$

where E_0 is the input energy bound defined in Section III-A. The resulting generalization gap for GNNSIC is therefore bounded by

$$\tilde{\mathcal{O}} \left(\frac{(\rho' + 1)}{T} (\bar{d}^{(\text{out})})^{\frac{1}{2}} (\bar{d}^{(\text{in})})^{\frac{N-1}{2}} \sqrt{E_0} \right), \quad (16)$$

where $\rho' = \bar{\rho}_{\text{inner}}$ due to parameter sharing. Compared with DeepSIC, the absence of depth-dependent growth in both A_G and B_G highlights the crucial role of parameter sharing in controlling the hypothesis space complexity.

The derived Rademacher complexity bounds expose a fundamental structural difference between DeepSIC and the proposed GNNSIC. For DeepSIC, the dominant terms in the bound grow exponentially with the number of SIC iterations, as a direct consequence of norm accumulation and degree

amplification induced by repeatedly composing non-shared neural modules along the outer DAG. In contrast, GNNSIC avoids this exponential growth by enforcing structured parameter sharing across both users and iterations, which effectively collapses the outer DAG and eliminates both effects. From a system design perspective, this analysis suggests that GNNSIC is particularly well suited for systems with a large number of users or deeper SIC iterations, where the exponential growth in model complexity inherent to conventional DeepSIC architectures may impose fundamental generalization limitations. By decoupling the generalization behavior from the number of SIC iterations, GNNSIC provides a theoretically grounded, more robust and generalizable framework for MIMO detection.

VI. NUMERICAL RESULTS

This section presents the performance evaluation of the proposed GNNSIC model compared with the baseline DeepSIC approach. For 6×6 case, all models are trained on 48,000 samples using the ADAM optimizer with a learning rate of 0.005, and validated on 12,000 samples. To ensure stable SER estimates, the number of testing samples increases with the Signal-to-Noise Ratio (SNR). Specifically, for the linear synthetic channel with SNR = 0 to 10 dB, 20,000 samples are used; in higher SNR regime, the number increases to 200,000 at 12 dB and 2,000,000 at 14 dB. Training is conducted over 100 epochs with a batch size of 64, while validation and testing use a batch size of 128. Binary phase-shift keying (BPSK) modulation is considered for simplicity, with $S = \{-1, +1\}$ and $M = 2$.

A. Linear Synthetic Channels

We first evaluate the proposed GNNSIC on a linear synthetic Gaussian channel, where the channel model and the CSI uncertainty follow exactly the settings for DeepSIC in [26]. In particular, we use *perfect CSI* to indicate training and testing on the same channel realization, while *CSI uncertainty* means training on a perturbed channel $\hat{h} = h + e$ with $e \sim \mathcal{N}(0, \sigma_e^2)$ and testing on the unperturbed channel h . All learning-based approaches are trained at 10 dB and tested at other SNRs for generalization evaluation.

As shown in Fig. 2, under perfect CSI, GNNSIC achieves performance comparable to that of *E2E DeepSIC*, and outperforms both iterative SIC and *Seq. DeepSIC*, demonstrating its ability to approximate DeepSIC's inference behavior within a structured message-passing framework. Within the entire SNR regime, GNNSIC closely follows the SER trajectory of *E2E DeepSIC*, with certain performance improvements at high SNRs. Under CSI uncertainty, both GNNSIC and DeepSIC exhibit strong robustness against channel perturbations, significantly outperforming the iterative SIC baseline. Notably, GNNSIC consistently yields lower SERs than *E2E DeepSIC* at all SNRs with or without CSI uncertainty, highlighting the enhanced generalization capability and robustness of GNNSIC.

B. Non-Linear Synthetic Channels

In this experiment, we evaluate the performance of GNNSIC on a non-linear synthetic channel against the baselines. This

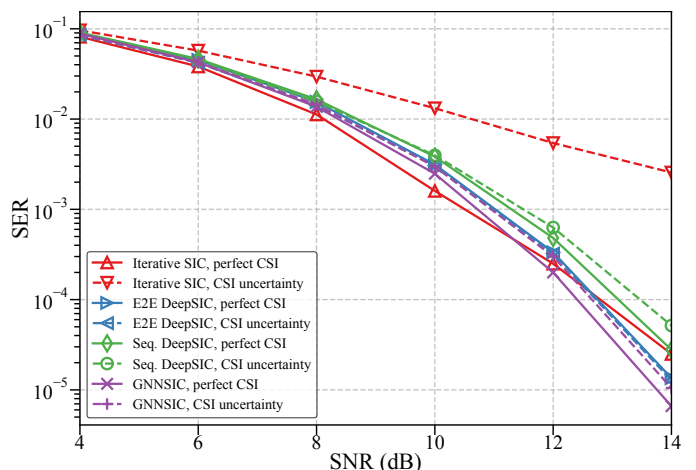


Fig. 2: SER performance versus SNR for GNNSIC, iterative SIC, and DeepSIC over a 6×6 linear Gaussian channel with perfect CSI ($\sigma_e^2 = 0$) and CSI uncertainty ($\sigma_e^2 = 0.1$).

setting aims to demonstrate that GNNSIC can achieve comparable performance to DeepSIC, even in quantized and Poisson communication scenarios, which are given in [26]. Since the sequential training variant of DeepSIC (i.e., *Seq. DeepSIC*) adopts the same network architecture as the end-to-end trained version (*E2E DeepSIC*) but exhibits inferior performance on synthetic linear Gaussian channels, we omit *Seq. DeepSIC* in subsequent comparisons and focus solely on *E2E DeepSIC*.

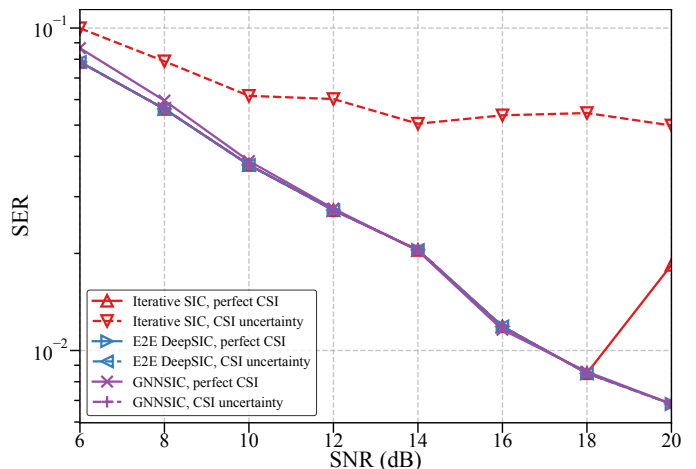


Fig. 3: SER versus SNR for GNNSIC, iterative SIC, and DeepSIC over a 4×4 synthetic quantized Gaussian channel with *perfect CSI* ($\sigma_e^2 = 0$) and *CSI uncertainty* ($\sigma_e^2 = 0.1$).

As illustrated in Fig. 3, GNNSIC achieves performance comparable to that of *E2E DeepSIC* under both perfect and imperfect CSI conditions in the quantized Gaussian channels. This indicates that GNNSIC is capable of effective symbol detection even in the presence of significant nonlinear distortions. The results for the Poisson channel are presented in Fig. 4, where GNNSIC achieves the lowest SER in all SNR regimes, significantly outperforming iterative SIC in the perfect CSI scenario. This highlights its superior capability in mitigating multiuser interference and enhancing detection

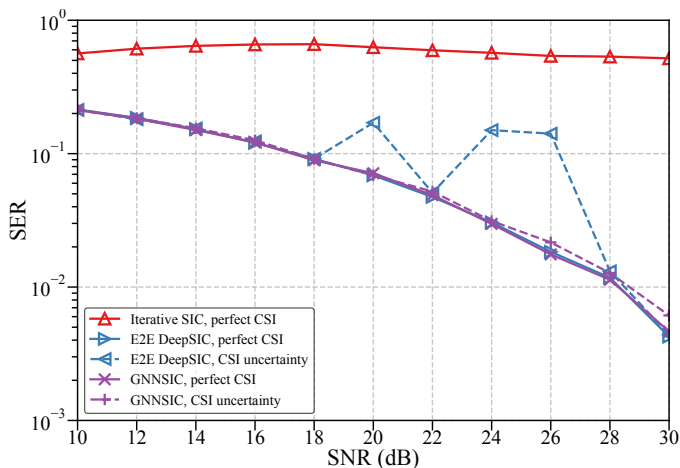


Fig. 4: SER versus SNR for GNNSIC, iterative SIC, and DeepSIC over a 4×4 synthetic Poisson channel with *perfect CSI* ($\sigma_e^2 = 0$) and *CSI uncertainty* ($\sigma_e^2 = 0.1$).

accuracy. Moreover, under CSI uncertainty, GNNSIC maintains a notable performance advantage, exhibiting reduced degradation compared to both iterative SIC and *E2E DeepSIC*. These results demonstrate the robustness of GNNSIC against channel estimation errors.

C. Robustness to CSI Uncertainty

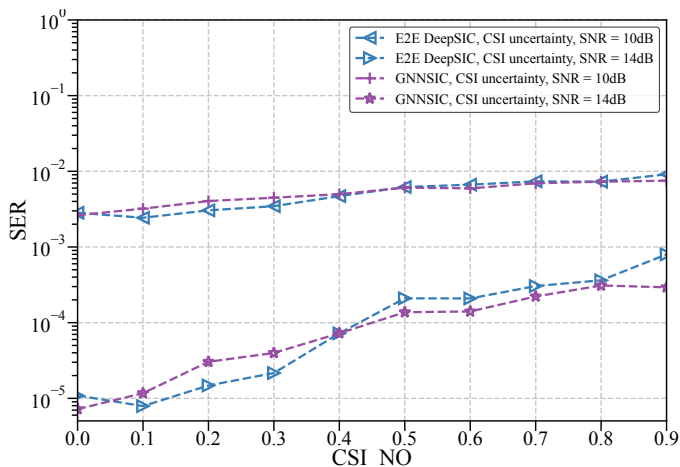


Fig. 5: SER versus CSI_NO for GNNSIC and DeepSIC at SNR = 10 dB and 14 dB on a 6×6 synthetic linear Gaussian channel.

To evaluate the robustness of GNNSIC and *E2E DeepSIC* under CSI uncertainty, we conduct experiments with varying levels of CSI noise (denoted as CSI_NO) at two fixed SNRs: 10 dB and 14 dB. As illustrated in Fig. 5, GNNSIC maintains as stable SER performance as DeepSIC when CSI uncertainty increases. At 10 dB SNR, the SER of both GNNSIC and DeepSIC increases slightly with CSI_NO. The effect of CSI uncertainty becomes more prominent at 14 dB, where both GNNSIC and DeepSIC experience significant performance degradation when CSI uncertainty increases. Notably, GNNSIC exhibits

a plateau in SER when CSI_NO values are high, indicating stronger resilience to severe CSI uncertainty.

D. User Generalization

Thanks to the advantage of cross-user parameter sharing, the proposed GNNSIC possesses excellent user generalization capability, that is, the trained GNNSIC model for a large number of users can be directly deployed to the MIMO scenarios with a small number of users *without re-training*. This is beyond the capability of DeepSIC, where the models should be *retrained* again and again for different user configurations.

This subsection investigates the user generalization capability of the proposed GNNSIC model in multiuser MIMO systems when the number of transmit users (K) varies. The GNNSIC detector is trained on a fixed 32×32 MIMO configuration, and is evaluated under different numbers of users, specifically $K = 8, 16, 32$. Comparative results are presented against both iterative SIC and DeepSIC baselines.

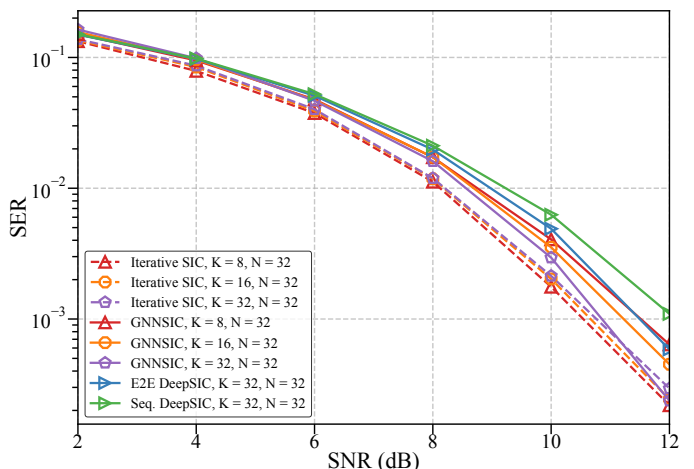


Fig. 6: User generalization performance of GNNSIC in terms of SER versus SNR on a synthetic linear Gaussian MIMO channel. The GNNSIC model is trained with $K = 32$ users and $N = 32$ antennas, and evaluated under different numbers of users ($K = 8, 16, 32$). Results are compared with the iterative SIC algorithm under matching K values. Additionally, the performance of DeepSIC under the 32×32 MIMO setting is provided for reference.

As illustrated in Fig. 6, the proposed GNNSIC model demonstrates excellent user generalization capability, maintaining consistent SER performance across different user configurations. For $K = 8, 16$, and 32 , GNNSIC achieves similar performance levels at low to moderate SNRs. As the number of users increases from $K = 8$ to $K = 32$, the performance gap between GNNSIC and iterative SIC gradually narrows. Notably, at $K = 32$, GNNSIC significantly outperforms DeepSIC and closely matches the performance of iterative SIC, even surpassing it in the high SNR regime (e.g., at SNR = 12 dB).

E. Sample Efficiency

The complexity comparison between DeepSIC and GNNSIC is summarized in Table I. Due to the cross-user

TABLE I: Numerical Comparison of Rademacher Complexity Terms for DeepSIC and GNNSIC over 6×6 MIMO.

Quantity	DeepSIC	GNNSIC
Number of blocks K	6	1 (shared)
Iterations	$L = 5$	$L = 1$ (shared)
MLP depth N	2	5
Constellation size M	2	2
$d_l^{(\text{out})}, d_l^{(\text{in})}$	(1), (30, 60)	(1), (14, 28, 2, 15, 28)
ρ	$\hat{\rho}_{\text{inner}}^L$	$\hat{\rho}_{\text{inner}}$
Generalization gap	$\mathcal{O}\left(\frac{K(\rho+1)}{T}\sqrt{A_D B_D}\right)$	$\mathcal{O}\left(\frac{(\rho+1)}{T}\sqrt{A_G B_G}\right)$
T for gap $\epsilon = 0.1$	$\sim 10^7$	$\sim 10^4$

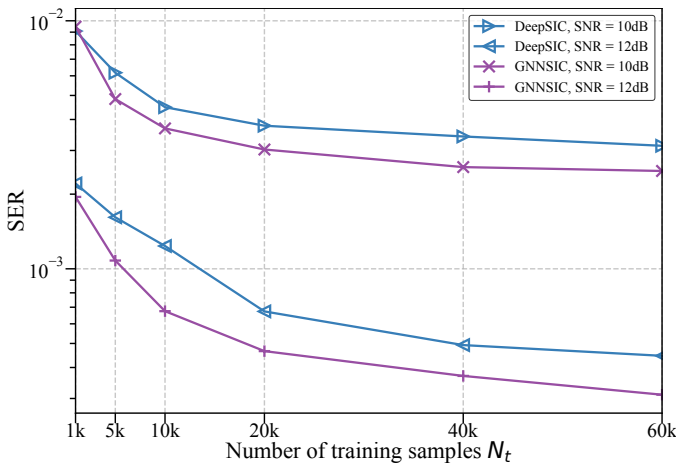


Fig. 7: SER versus the number of training samples for GNNSIC and DeepSIC at SNR = 10 dB and 12 dB over a 6×6 synthetic linear Gaussian channel.

and cross-iteration parameter sharing, GNNSIC admits a substantially smaller hypothesis class, leading to several orders-of-magnitude reduction in the worst-case generalization bound compared with DeepSIC.

It is important to emphasize that such a pronounced theoretical gap does not imply equally large differences in the empirical SER curves. This discrepancy is expected, since the derived bounds characterize worst-case deviations over the entire hypothesis class, whereas the trained networks correspond to specific low-norm solutions favored by stochastic first-order optimization under structured communication data. In the considered 6×6 MIMO setting with i.i.d. Gaussian channels and BPSK signaling, the underlying detection task is relatively simple, allowing even overparameterized architectures such as DeepSIC to generalize well when trained with sufficient data.

To further elucidate the improved sample efficiency observed in Fig. 7, Table II reports the number of trainable parameters of DeepSIC and GNNSIC under different MIMO configurations. Across all settings, GNNSIC consistently requires one to two orders of magnitude fewer parameters than DeepSIC, while preserving comparable expressivity through structured parameter sharing.

The substantially reduced model complexity translates into superior sample efficiency in practice. As shown in Fig. 7, GNNSIC achieves a target SER with significantly fewer train-

TABLE II: Trainable Parameters of Different Detectors

MIMO Setting	DeepSIC	GNNSIC
6×6	25,260	1,061
32×32	633,920	18,689
64×64	2,496,640	70,081

ing samples than DeepSIC at both SNR = 10 dB and 12 dB. For instance, at 10 dB, GNNSIC attains an SER of approximately 3.5×10^{-3} using only 10k training samples, whereas DeepSIC requires around 60k samples to reach comparable performance. Similar trends are observed at higher SNRs. These results confirm that the proposed architecture improves generalization by effectively controlling model complexity, rather than merely optimizing average-case performance.

VII. CONCLUSION

This paper studied fully data-driven MU-MIMO detection within a unified *Network-of-MLPs* framework, which models learning-based receivers as networks of MLP blocks interconnected by outer and inner DAGs. Within this framework, we reformulated soft interference cancellation as a graph-based message-passing process and proposed GNNSIC, which exploits parameter sharing across users and iterations. We further developed a norm-based generalization analysis for *Network-of-MLPs* using Rademacher complexity and DAG peeling, which reveals an exponential dependence of the generalization bound on the SIC depth for DeepSIC, eliminated in GNNSIC through parameter sharing. Simulation results demonstrate that GNNSIC attains comparable or improved SER performance with fewer parameters and training samples, while generalizing effectively across different user configurations.

APPENDIX

A. Proof of Lemma 2

For self-containedness, we provide a proof of Lemma 2, following the arguments of [43]. This lemma will be repeatedly instantiated in both the inner-level and outer-level peeling arguments developed in the subsequent sections.

Let $\mathbf{W}_j \in \mathbb{R}^{b \times p}$ denote its weight matrix, where b corresponds to the output dimension in the present setting, and write $\mathbf{w}_{j,1}^\top, \dots, \mathbf{w}_{j,b}^\top$ for its rows associated with the j -th output neuron. For notational convenience, define for any $\mathbf{a} \in \mathbb{R}^p$ the scalar functional

$$Q_j(\mathbf{a}) \triangleq \left(\sum_{t=1}^T \xi_t \sigma \left(\frac{\mathbf{a}^\top}{\|\mathbf{a}\|_2} f_j(\mathbf{x}_t) \right) \right)^2.$$

With this definition, a direct expansion yields

$$\begin{aligned} & \sum_{j=1}^q \left\| \sum_{t=1}^T \xi_t \sigma(\mathbf{W}_j f_j(\mathbf{x}_t)) \right\|_2^2 \\ &= \sum_{j=1}^q \sum_{\mu=1}^b \|\mathbf{w}_{j,\mu}\|_2^2 \left(\sum_{t=1}^T \xi_t \cdot \sigma \left(\frac{\mathbf{w}_{j,\mu}^\top}{\|\mathbf{w}_{j,\mu}\|_2} f_j(\mathbf{x}_t) \right) \right)^2 \end{aligned}$$

$$= \sum_{j=1}^q \sum_{\mu=1}^b \|\mathbf{w}_{j,\mu}\|_2^2 Q_j(\mathbf{w}_{j,\mu}).$$

For any collection $(\mathbf{w}_{j,\mu})_{\mu=1}^b$ satisfying $\|\mathbf{W}_j\|_F \leq R$, we clearly have

$$\sum_{\mu=1}^b \|\mathbf{w}_{j,\mu}\|_2^2 Q_j(\mathbf{w}_{j,\mu}) \leq R^2 \max_{\mu \in [b]} Q_j(\mathbf{w}_{j,\mu}). \quad (17)$$

The upper bound is attained by concentrating the entire Frobenius norm on a single row, namely by choosing $\hat{\mathbf{w}}_{j,\mu^*}$ with $\|\hat{\mathbf{w}}_{j,\mu^*}\|_2 = R$ for some $\mu^* \in [b]$ and setting all remaining rows to zero. Since g is monotone increasing, this implies

$$\begin{aligned} \mathbb{E}_\xi \sup_{\substack{f \in \mathcal{F} \\ \mathbf{W}_j: \|\mathbf{W}_j\|_F \leq R}} g \left(\sqrt{\sum_{j=1}^q \left\| \sum_{t=1}^T \xi_t \cdot \sigma(\mathbf{W}_j f_j(\mathbf{x}_t)) \right\|_2^2} \right) \\ \stackrel{(a)}{\leq} \mathbb{E}_\xi \sup_{\substack{f \in \mathcal{F} \\ \|\mathbf{w}_j\|_2 = R, j \in [q]}} g \left(\sqrt{\sum_{j=1}^q \left\| \sum_{t=1}^T \xi_t \cdot \sigma(\mathbf{w}_j^\top f_j(\mathbf{x}_t)) \right\|_2^2} \right) \\ \stackrel{(b)}{\leq} \mathbb{E}_\xi \sup_{j \in [q], f \in \mathcal{F}, \|\mathbf{w}\|_2 = R} g \left(\sqrt{q} \left\| \sum_{t=1}^T \xi_t \cdot \sigma(\mathbf{w}^\top f_j(\mathbf{x}_t)) \right\|_2 \right) \\ \stackrel{(c)}{\leq} 2 \mathbb{E}_\xi \sup_{j \in [q], f \in \mathcal{F}, \|\mathbf{w}\|_2 = R} g \left(\sqrt{q} \sum_{t=1}^T \xi_t \cdot \sigma(\mathbf{w}^\top f_j(\mathbf{x}_t)) \right) \\ \stackrel{(d)}{\leq} 2 \mathbb{E}_\xi \sup_{j \in [q], f \in \mathcal{F}} g \left(\sqrt{q} R \left\| \sum_{t=1}^T \xi_t f_j(\mathbf{x}_t) \right\|_2 \right), \quad (18) \end{aligned}$$

where (b) bounds the sum by its largest term, (c) uses the inequality $g(|z|) \leq g(z) + g(-z)$ together with the symmetry of the Rademacher variables $\{\xi_t\}$, and (d) follows from Equation (4.20) in [44] and the Cauchy–Schwarz inequality. This completes the proof. \blacksquare

B. Proof of Proposition 1

Fix an arbitrary function $f_w \in \mathcal{F}_{G,\rho}$, with ρ defined in (11). Let $\mathbf{W}_{k_l, j_n}^{(\text{in}), n} \in \mathbb{R}^{c_n \times (c_{n-1} |\text{pred}(n, j_n)_{k_l}|)}$ denote the weight matrix of the j_n -th channel-generating unit in layer n of the inner MLP for user $k \in [K]$ at outer iteration $l \in [L]$. Exploiting the positive homogeneity of ReLU, $\sigma(\alpha x) = \alpha \sigma(x)$, any $f_w \in \mathcal{F}_{G,\rho}$ admits an equivalent re-parameterization $f_{\hat{\mathbf{w}}}$ obtained by layerwise normalization.

For the inner MLPs, we normalize the output layer of the k -th block at iteration l as

$$\begin{aligned} \hat{\mathbf{W}}_{k_l}^{(\text{in}), N} &:= \bar{\rho}_{\text{inner}} \frac{\mathbf{W}_{k_l}^{(\text{in}), N}}{\|\mathbf{W}_{k_l}^{(\text{in}), N}\|_F}, \\ \hat{\mathbf{W}}_{k_l, j_n}^{(\text{in}), n} &:= \frac{\mathbf{W}_{k_l, j_n}^{(\text{in}), n}}{\max_{j_n} \|\mathbf{W}_{k_l, j_n}^{(\text{in}), n}\|_F}, \quad n < N. \end{aligned}$$

Similarly, for the outer network,

$$\begin{aligned} \hat{\mathbf{W}}^{(\text{out}), L} &:= \bar{\rho}_{\text{outer}} \frac{\mathbf{W}^{(\text{out}), L}}{\|\mathbf{W}^{(\text{out}), L}\|_F}, \\ \hat{\mathbf{W}}_{j_l}^{(\text{out}), l} &:= \frac{\mathbf{W}_{j_l}^{(\text{out}), l}}{\max_{j_l} \|\mathbf{W}_{j_l}^{(\text{out}), l}\|_F}, \quad l < L. \end{aligned}$$

By construction and the positive homogeneity of ReLU, the re-parameterized network $f_{\hat{\mathbf{w}}}$ realizes the same input–output mapping as f_w , and hence

$$\mathcal{F}_{G,\rho} \subseteq \hat{\mathcal{F}}_{G,\rho},$$

where

$$\begin{aligned} \hat{\mathcal{F}}_{G,\rho} := \left\{ f_{\hat{\mathbf{w}}} : \|\hat{\mathbf{W}}_{k_l}^{(\text{in}), N}\|_F \leq \bar{\rho}_{\text{inner}}, \right. \\ \left. \|\hat{\mathbf{W}}_{k_l, j_n}^{(\text{in}), n}\|_F \leq 1, \forall n < N, \right. \\ \left. \|\hat{\mathbf{W}}^{(\text{out}), L}\|_F \leq \bar{\rho}_{\text{outer}}, \|\hat{\mathbf{W}}_{j_l}^{(\text{out}), l}\|_F \leq 1 \right\}. \end{aligned}$$

It therefore suffices to bound the empirical Rademacher complexity $\mathcal{R}_{S_x}(\hat{\mathcal{F}}_{G,\rho})$. We consider the coordinate-wise complexity for the M -dimensional output and analyze the scaled quantity $TR_{S_x}(\hat{\mathcal{F}}_{G,\rho})$ via a peeling argument adapted to the multi-block, multi-iteration structure,

$$\begin{aligned} TR &:= TR_{S_x}(\hat{\mathcal{F}}_{G,\rho}) \\ &\stackrel{(a)}{=} \mathbb{E}_\xi \left[\sup_{\hat{\mathbf{w}}} \sum_{k=1}^K \sum_{t=1}^T \sum_{m=1}^M \xi_{k,t,m} f_{\hat{\mathbf{w}}}(\mathbf{x}_t)_{k,m} \right] \\ &\stackrel{(b)}{=} \mathbb{E}_\xi \left[\sup_{\hat{\mathbf{w}}} \sum_{k=1}^K \sum_{m=1}^M \sum_{t=1}^T \xi_{k,t,m} \right. \\ &\quad \cdot \left. \sum_{j_{N-1}} \langle \hat{\mathbf{W}}_{k_L, m, j_{N-1}}^{(\text{in}), N}, \mathbf{z}_{k_L, j_{N-1}}^{(\text{in}), N-1}(\mathbf{x}_t) \rangle \right] \\ &\stackrel{(c)}{=} \mathbb{E}_\xi \left[\sup_{\hat{\mathbf{w}}} \sum_{k=1}^K \sum_{j_{N-1}} \sum_{m=1}^M (\hat{\mathbf{W}}_{k_L, m, j_{N-1}}^{(\text{in}), N})^\top \right. \\ &\quad \cdot \left. \sum_{t=1}^T \xi_{k,t,m} \mathbf{z}_{k_L, j_{N-1}}^{(\text{in}), N-1}(\mathbf{x}_t) \right] \\ &\stackrel{(d)}{\leq} \bar{\rho}_{\text{inner}} \mathbb{E}_\xi \left[\sum_{k=1}^K \sup_{\hat{\mathbf{w}}} \max_{m, j_{N-1}} \left\| \sum_{t=1}^T \xi_{k,t,m} \mathbf{z}_{k_L, j_{N-1}}^{(\text{in}), N-1}(\mathbf{x}_t) \right\|_2 \right] \\ &\stackrel{(e)}{\leq} \bar{\rho}_{\text{inner}} \mathbb{E}_\xi \left[K \sup_{\hat{\mathbf{w}}} \max_{k_L, m, j_{N-1}} \left\| \sum_{t=1}^T \xi_{k_L, t, m} \mathbf{z}_{k_L, j_{N-1}}^{(\text{in}), N-1}(\mathbf{x}_t) \right\|_2 \right] \\ &\stackrel{(f)}{=} \bar{\rho}_{\text{inner}} K \mathbb{E}_\xi \left[\sup_{\hat{\mathbf{w}}} \max_{k_L, m, j_{N-1}} \left\| \sum_{t=1}^T \xi_{k_L, t, m} \mathbf{z}_{k_L, j_{N-1}}^{(\text{in}), N-1}(\mathbf{x}_t) \right\|_2 \right]. \quad (19) \end{aligned}$$

Here, k_L denotes the terminal block index after unrolling the outer iterations. Since each output coordinate corresponds to a unique terminal block, we relabel the maximization index accordingly. Step (d) follows from the Frobenius-norm constraint on the output-layer weights of the inner MLP, $\|\hat{\mathbf{W}}_{k_L}^{(\text{in}), N}\|_F \leq \bar{\rho}_{\text{inner}}$. By convexity, the supremum is attained by concentrating the norm on a single row of $\hat{\mathbf{W}}_{k_L}^{(\text{in}), N}$, and the bound follows from the Cauchy–Schwarz inequality.

To bound the expectation, we apply the log-sum-exp inequality together with Jensen’s inequality: for any $\lambda > 0$ and nonnegative random variable Z , $\mathbb{E}[Z] \leq \lambda^{-1} \log \mathbb{E}[\exp(\lambda Z)]$. This yields

$$\mathbb{E}_\xi \left[\sup_{\hat{\mathbf{w}}} \max_{k_L, m, j_{N-1}} \left\| \sum_{t=1}^T \xi_{k_L, t, m} \mathbf{z}_{k_L, j_{N-1}}^{(\text{in}), N-1}(\mathbf{x}_t) \right\|_2 \right]$$

$$\begin{aligned}
&\leq \frac{1}{\lambda} \log \mathbb{E}_\xi \sup_{\substack{\hat{\mathbf{w}}, k_L, m, \\ j_{N-1}}} \exp \left(\lambda \left\| \sum_{t=1}^T \xi_{k_L, t, m} \mathbf{z}_{k_L, j_{N-1}}^{(\text{in}), N-1}(\mathbf{x}_t) \right\|_2 \right) \\
&= \frac{1}{\lambda} \log \mathbb{E}_\xi \sup_{\substack{\hat{\mathbf{w}}, k_L, m, \\ j_{N-1}}} \exp \left(\lambda \sqrt{\left\| \sum_{t=1}^T \xi_{k_L, t, m} \mathbf{z}_{k_L, j_{N-1}}^{(\text{in}), N-1}(\mathbf{x}_t) \right\|_2^2} \right). \tag{20}
\end{aligned}$$

We then recursively apply the peeling argument of Lemma 2 with $g(x) = \exp(\lambda x)$. This is valid since the normalized weights satisfy $\|\hat{\mathbf{W}}_{k_l, j_n}^{(\text{in}), n}\|_F \leq 1$ and the ReLU activation is positively homogeneous and 1-Lipschitz. Starting from layer $N-1$, we obtain

$$\begin{aligned}
&\mathbb{E}_\xi \sup_{\substack{\hat{\mathbf{w}}, k_L, m, \\ j_{N-1}}} \exp \left(\lambda \sqrt{\left\| \sum_{t=1}^T \xi_{k_L, t, m} \mathbf{z}_{k_L, j_{N-1}}^{(\text{in}), N-1}(\mathbf{x}_t) \right\|_2^2} \right) \\
&\stackrel{(a)}{=} \mathbb{E}_\xi \sup_{\substack{\hat{\mathbf{w}}, k_L, m, \\ j_{N-1}}} \exp \left(\lambda \sqrt{\left\| \sum_{t=1}^T \xi_{k_L, t, m} \sigma(\hat{\mathbf{W}}_{k_L, j_{N-1}}^{(\text{in}), N-1} \mathbf{v}_{k_L, j_{N-1}}^{(\text{in}), N-2}(\mathbf{x}_t)) \right\|_2^2} \right) \\
&\stackrel{(b)}{\leq} 2 \mathbb{E}_\xi \sup_{\substack{\hat{\mathbf{w}}, k_L, m, \\ j_{N-1}}} \exp \left(\lambda \sqrt{\left\| \sum_{t=1}^T \xi_{k_L, t, m} \mathbf{v}_{k_L, j_{N-1}}^{(\text{in}), N-2}(\mathbf{x}_t) \right\|_2^2} \right) \\
&\stackrel{(c)}{=} 2 \mathbb{E}_\xi \sup_{\substack{\hat{\mathbf{w}}, k_L, m, \\ j_{N-1}}} \exp \left(\lambda \left[\sum_{j_{N-2} \in \text{pred}(N-1, j_{N-1})_{k_L}} \left\| \sum_{t=1}^T \xi_{k_L, t, m} \right. \right. \right. \\
&\quad \left. \left. \left. \cdot \sigma(\hat{\mathbf{W}}_{k_L, j_{N-2}}^{(\text{in}), N-2} \mathbf{v}_{k_L, j_{N-2}}^{(\text{in}), N-3}(\mathbf{x}_t)) \right\|_2 \right]^{\frac{1}{2}} \right) \\
&\stackrel{(d)}{\leq} 4 \mathbb{E}_\xi \sup_{\substack{\hat{\mathbf{w}}, k_L, m, \\ j_{N-1}, j_{N-2}}} \exp \left(\lambda \left[|\text{pred}(N-1, j_{N-1})_{k_L}| \right. \right. \\
&\quad \left. \left. \cdot \left\| \sum_{t=1}^T \xi_{k_L, t, m} \mathbf{v}_{k_L, j_{N-2}}^{(\text{in}), N-3}(\mathbf{x}_t) \right\|_2 \right]^{\frac{1}{2}} \right) \\
&\stackrel{(f)}{\leq} 2^N \mathbb{E}_\xi \max_{\substack{k_L, m, \\ j_0, \dots, j_N}} \exp \left(\lambda \left[\prod_{n=1}^{N-1} |\text{pred}(n, j_n)_{k_L}| \right. \right. \\
&\quad \left. \left. \cdot \left\| \sum_{t=1}^T \xi_{k_L, t, m} \mathbf{z}_{k_L, j_0}^{(\text{in}), 0}(\mathbf{x}_t) \right\|_2 \right]^{\frac{1}{2}} \right) \\
&\stackrel{(h)}{\leq} 2^N \mathbb{E}_\xi \max_{\substack{\hat{\mathbf{w}}, k_L, m, \\ j_0, \dots, j_N}} \exp \left(\lambda \left[\prod_{n=1}^{N-1} |\text{pred}(n, j_n)_{k_L}| \right. \right. \\
&\quad \left. \left. \cdot \left\| \sum_{t=1}^T \xi_{k_L, t, m} \sigma(\hat{\mathbf{W}}_{k_L}^{(\text{out}), L} \mathbf{v}_{k_L}^{(\text{out}), L-1}(\mathbf{x}_t)) \right\|_2 \right]^{\frac{1}{2}} \right) \\
&\stackrel{(j)}{\leq} 2^{N+1} \mathbb{E}_\xi \max_{\substack{\hat{\mathbf{w}}, m, \\ j_0, \dots, j_N, \\ k_L}} \exp \left(\lambda \bar{\rho}_{\text{outer}} \sqrt{\prod_{n=1}^{N-1} |\text{pred}(n, j_n)_{k_L}|} \right. \\
&\quad \left. \cdot \left\| \sum_{t=1}^T \xi_{k_L, t, m} \mathbf{v}_{k_L}^{(\text{out}), L-1}(\mathbf{x}_t) \right\|_2 \right)
\end{aligned}$$

$$\begin{aligned}
&\stackrel{(j)}{\leq} 2^{N+1} \mathbb{E}_\xi \max_{\substack{\hat{\mathbf{w}}, m, \\ j_0, \dots, j_N, \\ k_L, k_{L-1}}} \exp \left(\lambda \bar{\rho}_{\text{outer}} \right. \\
&\quad \cdot \sqrt{\prod_{n=1}^{N-1} |\text{pred}(n, j_n)_{k_L}| \cdot |\text{pred}(L, k_L)|} \\
&\quad \left. \cdot \left\| \sum_{t=1}^T \xi_{k_L, t, m} \mathbf{z}_{k_{L-1}}^{(\text{out}), L-1}(\mathbf{x}_t) \right\|_2 \right) \\
&\stackrel{(k)}{\leq} 2^{(N+1)L} \mathbb{E}_\xi \max_{\substack{m, j_0, \dots, j_N \\ k_0, \dots, k_L}} \exp \left(\lambda \bar{\rho}_{\text{outer}} (\bar{\rho}_{\text{inner}})^{L-1} \right. \\
&\quad \cdot \sqrt{\prod_{l=1}^L |\text{pred}(l, k_l)| \cdot \prod_{l=1}^L \prod_{n=1}^{N-1} |\text{pred}(n, j_n)_{k_l}|} \\
&\quad \left. \cdot \left\| \sum_{t=1}^T \xi_{k_L, t, m} \mathbf{z}_{k_0}^{(\text{out}), 0}(\mathbf{x}_t) \right\|_2 \right). \tag{21}
\end{aligned}$$

Here, (f) follows from recursively applying the peeling argument over the N -layer inner MLPs, while (h)–(j) result from applying Peeling Lemma 2 to the outer network. Step (k) is obtained by iterating the outer peeling process over L blocks. The maximization is taken over all valid unit-level paths (j_0, \dots, j_N) and block-level paths (k_0, \dots, k_L) satisfying $j_{n-1} \in \text{pred}(n, j_n)_{k_l}$ and $k_{l-1} \in \text{pred}(l, k_l)$. Since all index sets are finite, the supremum reduces to a maximum. Each block outputs an M -dimensional vector, yielding a factor M^L via a union bound over output coordinates. We notice that:

$$\begin{aligned}
&\mathbb{E}_\xi \max_{m, j_0, \dots, j_N} \max_{k_0, \dots, k_L} \exp \left(\lambda \bar{\rho}_{\text{outer}} (\bar{\rho}_{\text{inner}})^{L-1} \right. \\
&\quad \cdot \sqrt{\prod_{l=1}^L |\text{pred}(l, k_l)| \cdot \prod_{l=1}^L \left(\prod_{n=1}^{N-1} |\text{pred}(n, j_n)_{k_l}| \right)} \\
&\quad \left. \cdot \left\| \sum_{t=1}^T \xi_{k_L, t, m} \mathbf{z}_{k_0}^{(\text{out}), 0}(\mathbf{x}_t) \right\|_2 \right) \\
&\leq \sum_{m, j_0, \dots, j_N} \sum_{k_0, \dots, k_L} \mathbb{E}_\xi \exp \left(\lambda \bar{\rho}_{\text{outer}} (\bar{\rho}_{\text{inner}})^{L-1} \right. \\
&\quad \cdot \sqrt{\prod_{l=1}^L |\text{pred}(l, k_l)| \cdot \prod_{l=1}^L \left(\prod_{n=1}^{N-1} |\text{pred}(n, j_n)_{k_l}| \right)} \\
&\quad \left. \cdot \left\| \sum_{t=1}^T \xi_{k_L, t, m} \mathbf{z}_{k_0}^{(\text{out}), 0}(\mathbf{x}_t) \right\|_2 \right) \\
&\leq M^L \prod_{l=1}^L \left(\prod_{n=1}^{N-1} d_{l, n}^{(\text{in})} \right) \cdot \prod_{l=1}^L d_l^{(\text{out})} \max_{m, j_0, \dots, j_N} \max_{k_0, \dots, k_L} \mathbb{E}_\xi \\
&\quad \exp \left(\lambda \bar{\rho}_{\text{outer}} (\bar{\rho}_{\text{inner}})^{L-1} \right. \\
&\quad \left. \cdot \sqrt{\prod_{l=1}^L |\text{pred}(l, k_l)| \cdot \prod_{l=1}^L \left(\prod_{n=1}^{N-1} |\text{pred}(n, j_n)_{k_l}| \right)} \right)
\end{aligned}$$

$$\cdot \left\| \sum_{t=1}^T \xi_{k_L, t, m} \mathbf{z}_{k_0}^{(\text{out}), 0}(\mathbf{x}_t) \right\|_2. \quad (22)$$

By combining the peeling bounds with exponential-moment arguments, the empirical Rademacher complexity admits:

$$\begin{aligned} & T\mathcal{R}_{S_x}(\hat{\mathcal{F}}_{G, \bar{\rho}}) \\ & \leq \bar{\rho}_{\text{inner}} K \mathbb{E}_{\xi} \left[\sup_{\hat{\mathbf{w}}} \max_{\substack{k_L, m, \\ j_{N-1}}} \left\| \sum_{t=1}^T \xi_{k_L, t, m} \mathbf{z}_{k_L, j_{N-1}}^{(\text{in}), N-1}(\mathbf{x}_t) \right\|_2 \right] \\ & \leq \frac{\bar{\rho}_{\text{inner}} K}{\lambda} \log \left(2^{(N+1)L} M^L \prod_{l=1}^L \left(\prod_{n=1}^{N-1} d_{l,n}^{(\text{in})} \right) \prod_{l=1}^L d_l^{(\text{out})} \right) \\ & \quad \cdot \max_{m, j_0, \dots, j_N} \max_{k_0, \dots, k_L} \mathbb{E}_{\xi} \exp \left(\lambda \bar{\rho}_{\text{outer}} (\bar{\rho}_{\text{inner}})^{L-1} \right. \\ & \quad \cdot \sqrt{\prod_{l=1}^L |\text{pred}(l, k_l)| \prod_{l=1}^L \left(\prod_{n=1}^{N-1} |\text{pred}(n, j_n)_{k_l}| \right)} \\ & \quad \left. \cdot \left\| \sum_{t=1}^T \xi_{k_L, t, m} \mathbf{z}_{k_0}^{(\text{out}), 0}(\mathbf{x}_t) \right\|_2 \right). \quad (23) \end{aligned}$$

The remaining expectation is of the form $\mathbb{E}_{\xi} \exp(\alpha \|\sum_{t=1}^T \xi_t \mathbf{z}_t\|_2)$. By standard sub-Gaussian concentration (e.g., [45, Thm. 6.2]), for any $\alpha > 0$,

$$\begin{aligned} & \mathbb{E}_{\xi} \exp \left(\alpha \left\| \sum_{t=1}^T \xi_{k_L, t, m} \mathbf{z}_{j_0}^0(\mathbf{x}_t) \right\|_2 \right) \\ & \leq \exp \left(\frac{\alpha^2}{2} \sum_{t=1}^T \|\mathbf{z}_{k_0}^{(\text{out}), 0}(\mathbf{x}_t)\|_2^2 + \alpha \sqrt{\sum_{t=1}^T \|\mathbf{z}_{k_0}^{(\text{out}), 0}(\mathbf{x}_t)\|_2^2} \right). \quad (24) \end{aligned}$$

By combining (19)–(24) and setting

$$\alpha = \lambda \bar{\rho}_{\text{outer}} (\bar{\rho}_{\text{inner}})^{L-1} \sqrt{\prod_{l=1}^L |\text{pred}(l, k_l)| \prod_{l=1}^L \prod_{n=1}^{N-1} |\text{pred}(n, j_n)_{k_l}|},$$

we obtain the following bound:

$$\begin{aligned} & T\mathcal{R}_{S_x}(\hat{\mathcal{F}}_{G, \bar{\rho}}) \\ & \leq \frac{\bar{\rho}_{\text{inner}} K}{\lambda} \left[(N+1)L \log 2 + L \log M \right. \\ & \quad \left. + \sum_{l=1}^L \log d_l^{(\text{out})} + \sum_{l=1}^L \sum_{n=1}^{N-1} \log d_{l,n}^{(\text{in})} \right] \\ & \quad + \frac{\lambda K}{2} \bar{\rho}_{\text{outer}}^2 (\bar{\rho}_{\text{inner}})^{2(L-1)} \max_{k_0, \dots, k_L} \prod_{l=1}^L |\text{pred}(l, k_l)| \\ & \quad \cdot \max_{j_0, \dots, j_N} \prod_{l=1}^L \prod_{n=1}^{N-1} |\text{pred}(n, j_n)_{k_l}| \max_{k_0} \sum_{t=1}^T \|\mathbf{z}_{k_0}^{(\text{out}), 0}(\mathbf{x}_t)\|_2^2 \\ & \quad + K \bar{\rho}_{\text{outer}} (\bar{\rho}_{\text{inner}})^L \left[\max_{k_0, \dots, k_L} \prod_{l=1}^L |\text{pred}(l, k_l)| \right. \\ & \quad \left. \cdot \max_{j_0, \dots, j_N} \prod_{l=1}^L \prod_{n=1}^{N-1} |\text{pred}(n, j_n)_{k_l}| \max_{k_0} \sum_{t=1}^T \|\mathbf{z}_{k_0}^{(\text{out}), 0}(\mathbf{x}_t)\|_2^2 \right]^{\frac{1}{2}}. \quad (25) \end{aligned}$$

Optimizing the bound with respect to λ yields

$$\begin{aligned} \lambda = & \left[2 \left((N+1)L \log 2 + L \log M + \sum_{l=1}^L \log d_l^{(\text{out})} \right. \right. \\ & \left. \left. + \sum_{l=1}^L \sum_{n=1}^{N-1} \log d_{l,n}^{(\text{in})} \right) \right] / \left(\bar{\rho}_{\text{inner}}^{2(L-1)} \bar{\rho}_{\text{outer}}^2 \right) \\ & \cdot \max_{k_0, \dots, k_L} \prod_{l=1}^L |\text{pred}(l, k_l)| \max_{j_0, \dots, j_N} \prod_{l=1}^L \prod_{n=1}^{N-1} |\text{pred}(n, j_n)_{k_l}| \\ & \cdot \max_{k_0} \sum_{t=1}^T \|\mathbf{z}_{k_0}^{(\text{out}), 0}(\mathbf{x}_t)\|_2^2 \Big]^{\frac{1}{2}}. \end{aligned}$$

Substituting this choice of λ into (25) completes the proof. ■

C. Proof of Theorem 1

For $r \in \mathbb{N} \cup \{0\}$, define function class $\mathcal{F}_{G,r}$. We assign a failure probability budget

$$\delta_r := \frac{\delta}{r(r+1)}, \quad r \geq 1,$$

which satisfies $\sum_{r \geq 1} \delta_r = \delta$.

By Lemma 1, for any fixed shell index r , the following inequality holds with probability at least $1 - \delta_r$:

$$\text{err}_P(\mathbf{w}) - \text{err}_S^\gamma(\mathbf{w}) \leq \frac{2\sqrt{2}}{\gamma} \mathcal{R}_{S_x}(\mathcal{F}_{G,r}) + 3\sqrt{\frac{\log(2/\delta_r)}{2T}}. \quad (26)$$

Substituting the Rademacher complexity upper bound from Proposition 1, we introduce the shorthand notation

$$\begin{aligned} A & := (N+1)L \log 2 + L \log M \\ & \quad + \sum_{l=1}^L \log d_l^{(\text{out})} + \sum_{l=1}^L \sum_{n=1}^{N-1} \log d_{l,n}^{(\text{in})}, \\ B & := \max_{k_0, \dots, k_L} \prod_{l=1}^L |\text{pred}(l, k_l)| \max_{j_0, \dots, j_N} \prod_{l=1}^L \prod_{n=1}^{N-1} |\text{pred}(n, j_n)_{k_l}| \\ & \quad \cdot \max_{k_0} \sum_{t=1}^T \|\mathbf{z}_{k_0}^{(\text{out}), 0}(\mathbf{x}_t)\|_2^2. \end{aligned}$$

Proposition 1, together with the uniform inner-block bound $\bar{\rho}_{\text{inner}}$ and outer-block bound $\bar{\rho}_{\text{outer}}$, yields

$$\mathcal{R}_{S_x}(\mathcal{F}_{G,r}) \leq \frac{\bar{\rho}_{\text{inner}}^L \bar{\rho}_{\text{outer}} K}{T} (1 + \sqrt{2A}) \sqrt{B}.$$

Plugging this bound into (26) implies that, with probability at least $1 - \delta_r$,

$$\begin{aligned} \text{err}_P(\mathbf{w}) - \text{err}_S^\gamma(\mathbf{w}) & \leq \frac{2\sqrt{2} K \bar{\rho}_{\text{inner}}^L \bar{\rho}_{\text{outer}}}{\gamma T} (1 + \sqrt{2A}) \sqrt{B} \\ & \quad + 3\sqrt{\frac{\log(2/\delta_r)}{2T}}. \end{aligned}$$

Applying the union bound over all $r \geq 1$ (since $\sum_r \delta_r = \delta$), the above inequality holds uniformly for all parameter settings with probability at least $1 - \delta$. For any $f_{\mathbf{w}} \in \mathcal{F}_{G,r}$ with norm

$\rho(\mathbf{w})$, which is upper-bounded by $\bar{\rho}_{\text{inner}}^L \bar{\rho}_{\text{outer}}$, we choose $r = \lceil \rho(\mathbf{w}) \rceil \geq 1$. Noting that

$$\log\left(\frac{2}{\delta_r}\right) = \log\left(\frac{2r(r+1)}{\delta}\right) \leq \log\left(\frac{2(r+1)^2}{\delta}\right), r \leq \rho(\mathbf{w}) + 1,$$

we obtain that, with probability at least $1 - \delta$,

$$\begin{aligned} \text{err}_P(\mathbf{w}) - \text{err}_S^{\gamma}(\mathbf{w}) &\leq \frac{2\sqrt{2}K \lceil \rho(\mathbf{w}) \rceil (1 + \sqrt{2A})\sqrt{B}}{\gamma T} \\ &\quad + 3\sqrt{\frac{\log(2 \lceil \rho(\mathbf{w}) \rceil (\lceil \rho(\mathbf{w}) \rceil + 1)/\delta)}{2T}} \\ &\leq \frac{2\sqrt{2}K (\rho(\mathbf{w}) + 1) (1 + \sqrt{2A})\sqrt{B}}{\gamma T} \\ &\quad + 3\sqrt{\frac{\log(2(\rho(\mathbf{w}) + 2)^2/\delta)}{2T}}, \end{aligned} \quad (27)$$

which completes the proof. \blacksquare

REFERENCES

- [1] Y. Yi, X. Yi, W. Wang, and S. Jin, "GNNSIC: A New Approach to Soft Interference Cancellation with Graph Neural Networks," in *2025 IEEE/CIC International Conference on Communications in China (ICCC)*, 2025, pp. 1–6.
- [2] G. J. Foschini and M. J. Gans, "On Limits of Wireless Communications in a Fading Environment when Using Multiple Antennas," *Wireless personal communications*, vol. 6, pp. 311–335, 1998.
- [3] T. L. Marzetta, "Noncooperative Cellular Wireless with Unlimited Numbers of Base Station Antennas," *IEEE transactions on wireless communications*, vol. 9, no. 11, pp. 3590–3600, 2010.
- [4] A. Paulraj, R. Nabar, and D. Gore, *Introduction to Space-Time Wireless Communications*. Cambridge university press, 2003.
- [5] A. El Gamal and Y.-H. Kim, *Network Information Theory*. Cambridge university press, 2011.
- [6] J. G. Andrews, "Interference cancellation for cellular systems: a contemporary overview," *IEEE Wireless Communications*, vol. 12, no. 2, pp. 19–29, 2005.
- [7] E. Che, H. D. Tuan, H. H. M. Tam, and H. H. Nguyen, "Successive Interference Mitigation in Multiuser MIMO Channels," *IEEE Transactions on Communications*, vol. 63, no. 6, pp. 2185–2199, 2015.
- [8] W.-J. Choi, K.-W. Cheong, and J. Cioffi, "Iterative soft interference cancellation for multiple antenna systems," in *2000 IEEE Wireless Communications and Networking Conference. Conference Record (Cat. No.00TH8540)*, vol. 1, 2000, pp. 304–309 vol.1.
- [9] X. Wang and H. V. Poor, "Iterative (turbo) soft interference cancellation and decoding for coded CDMA," *IEEE transactions on communications*, vol. 47, no. 7, pp. 1046–1061, 1999.
- [10] P. Alexander, M. Reed, J. Asenstorfer, and C. Schlegel, "Iterative multiuser interference reduction: turbo CDMA," *IEEE Transactions on Communications*, vol. 47, no. 7, pp. 1008–1014, 1999.
- [11] N. Shlezinger, J. Whang, Y. C. Eldar, and A. G. Dimakis, "Model-Based Deep Learning," *Proceedings of the IEEE*, vol. 111, no. 5, pp. 465–499, 2023.
- [12] W. Yu, Y. Ma, H. He, S. Song, J. Zhang, and K. B. Letaief, "Deep Learning for Near-Field XL-MIMO Transceiver Design: Principles and Techniques," *IEEE Communications Magazine*, vol. 63, no. 1, pp. 52–58, 2025.
- [13] H. He, C.-K. Wen, S. Jin, and G. Y. Li, "Model-Driven Deep Learning for MIMO Detection," *IEEE Transactions on Signal Processing*, vol. 68, pp. 1702–1715, 2020.
- [14] J. Ma and L. Ping, "Orthogonal AMP," *IEEE Access*, vol. 5, pp. 2020–2033, 2017.
- [15] M. Khani, M. Alizadeh, J. Hoydis, and P. Fleming, "Adaptive neural signal detection for massive mimo," *IEEE Transactions on Wireless Communications*, vol. 19, no. 8, pp. 5635–5648, 2020.
- [16] A. Kosasih, V. Onasis, V. Miloslavskaya, W. Hardjajawana, V. Andrean, and B. Vucetic, "Graph Neural Network Aided MU-MIMO Detectors," *IEEE Journal on Selected Areas in Communications*, vol. 40, no. 9, pp. 2540–2555, 2022.
- [17] X. Zhou, J. Zhang, C.-K. Wen, S. Jin, and S. Han, "Graph Neural Network-Enhanced Expectation Propagation Algorithm for MIMO Turbo Receivers," *IEEE Transactions on Signal Processing*, vol. 71, pp. 3458–3473, 2023.
- [18] J. Cespedes, P. M. Olmos, M. Sánchez-Fernández, and F. Perez-Cruz, "Expectation Propagation Detection for High-Order High-Dimensional MIMO Systems," *IEEE Trans. Commun.*, vol. 62, no. 8, pp. 2840–2849, Aug. 2014.
- [19] H. He, X. Yu, J. Zhang, S. Song, and K. B. Letaief, "Message Passing Meets Graph Neural Networks: A New Paradigm for Massive MIMO Systems," *IEEE Transactions on Wireless Communications*, vol. 23, no. 5, pp. 4709–4723, 2024.
- [20] C. Jeon, R. Ghods, A. Maleki, and C. Studer, "Optimality of Large MIMO Detection via Approximate Message Passing," in *Proc. IEEE Int. Symp. Inf. Theory (ISIT)*, Hong Kong, Jun. 2015, pp. 1227–1231.
- [21] N. Samuel, T. Diskin, and A. Wiesel, "Learning to Detect," *IEEE Transactions on Signal Processing*, vol. 67, no. 10, pp. 2554–2564, 2019.
- [22] N. Shlezinger, N. Farsad, Y. C. Eldar, and A. J. Goldsmith, "ViterbiNet: A Deep Learning Based Viterbi Algorithm for Symbol Detection," *IEEE Transactions on Wireless Communications*, vol. 19, no. 5, pp. 3319–3331, 2020.
- [23] K. Pratik, B. D. Rao, and M. Welling, "RE-MIMO: Recurrent and Permutation Equivariant Neural MIMO Detection," *IEEE Transactions on Signal Processing*, vol. 69, pp. 459–473, 2021.
- [24] H. Ye and L. Liang, "On Purely Data-Driven Massive MIMO Detectors," *IEEE Transactions on Signal Processing*, vol. 73, pp. 3079–3093, 2025.
- [25] J. Hong, L. Liu, X. Bian, W. Wang, and Z. Zhang, "Soft Graph Transformer for MIMO Detection," 2026. [Online]. Available: <https://arxiv.org/abs/2509.12694>
- [26] N. Shlezinger, R. Fu, and Y. C. Eldar, "DeepSIC: Deep Soft Interference Cancellation for Multiuser MIMO Detection," *IEEE Transactions on Wireless Communications*, vol. 20, no. 2, pp. 1349–1362, 2020.
- [27] T. Raviv, S. Park, O. Simeone, Y. C. Eldar, and N. Shlezinger, "Online meta-learning for hybrid model-based deep receivers," *IEEE Transactions on Wireless Communications*, vol. 22, no. 10, pp. 6415–6431, 2023.
- [28] T. Raviv and N. Shlezinger, "Modular hypernetworks for scalable and adaptive deep mimo receivers," *IEEE Open Journal of Signal Processing*, vol. 6, pp. 256–265, 2025.
- [29] N. Weinberger, "Generalization bounds and algorithms for learning to communicate over additive noise channels," *IEEE Transactions on Information Theory*, vol. 68, no. 3, pp. 1886–1921, 2022.
- [30] A. Tsvieli and N. Weinberger, "Learning maximum margin channel decoders," *IEEE Transactions on Information Theory*, vol. 69, no. 6, pp. 3597–3626, 2023.
- [31] S. Adiga, X. Xiao, R. Tandon, B. Vasić, and T. Bose, "Generalization bounds for neural belief propagation decoders," *IEEE Transactions on Information Theory*, vol. 70, no. 6, pp. 4280–4296, 2024.
- [32] Q. Hu, F. Gao, H. Zhang, G. Y. Li, and Z. Xu, "Understanding Deep MIMO Detection," *IEEE Transactions on Wireless Communications*, vol. 22, no. 12, pp. 9626–9639, 2023.
- [33] B. Neyshabur, R. Tomioka, and N. Srebro, "Norm-Based Capacity Control in Neural Networks," in *Proc. Conf. Learn. Theory (COLT)*, Paris, France, Jul. 2015, pp. 1376–1401.
- [34] N. Golowich, A. Rakhlin, and O. Shamir, "Size-Independent Sample Complexity of Neural Networks," *Inf. Inference*, vol. 9, no. 2, pp. 473–504, May 2020.
- [35] P. L. Bartlett and S. Mendelson, "Rademacher and Gaussian Complexities: Risk Bounds and Structural Results," *J. Mach. Learn. Res.*, vol. 3, pp. 463–482, Nov. 2002.
- [36] N. Harvey, C. Liaw, and A. Mehrabian, "Nearly-Tight VC-Dimension and Pseudodimension Bounds for Piecewise Linear Neural Networks," in *Proc. Conf. Learn. Theory (COLT)*, Amsterdam, Netherlands, Jul. 2017, pp. 1064–1068.
- [37] P. L. Bartlett, D. J. Foster, and M. Telgarsky, "Spectrally-Normalized Margin Bounds for Neural Networks," in *Proc. Adv. Neural Inf. Process. Syst. (NeurIPS)*, Long Beach, CA, USA, Dec. 2017, pp. 6240–6249.
- [38] Y. Cao and Q. Gu, "Generalization Bounds of Stochastic Gradient Descent for Wide and Deep Neural Networks," in *Proc. Adv. Neural Inf. Process. Syst. (NeurIPS)*, Vancouver, BC, Canada, Dec. 2019, pp. 10 836–10 846.
- [39] A. Daniely and E. Granot, "Generalization Bounds for Neural Networks via Approximate Description Length," in *Proc. Adv. Neural Inf. Process. Syst. (NeurIPS)*, Vancouver, BC, Canada, Dec. 2019, pp. 13 009–13 017.
- [40] C. Wei and T. Ma, "Data-Dependent Sample Complexity of Deep Neural Networks via Lipschitz Augmentation," in *Proc. Adv. Neural Inf. Process. Syst. (NeurIPS)*, Vancouver, BC, Canada, Dec. 2019, pp. 9722–9733.

- [41] M. Mohri, A. Rostamizadeh, and A. Talwalkar, *Foundations of Machine Learning*, 2nd ed. Cambridge, MA, USA: MIT Press, 2018.
- [42] S. Shalev-Shwartz and S. Ben-David, *Understanding Machine Learning: From Theory to Algorithms*. Cambridge, U.K.: Cambridge Univ. Press, 2014.
- [43] T. Galanti, M. Xu, L. Galanti, and T. Poggio, “Norm-based Generalization Bounds for Sparse Neural Networks,” *Advances in Neural Information Processing Systems*, vol. 36, pp. 42 482–42 501, 2023.
- [44] M. Ledoux and M. Talagrand, *Probability in Banach Spaces*. Berlin, Germany: Springer, 1991.
- [45] S. Boucheron, G. Lugosi, and P. Massart, *Concentration Inequalities: A Nonasymptotic Theory of Independence*. Oxford, U.K.: Oxford Univ. Press, 2013.